Synthesis and characterization of zinc substituted Hydroxyapatite extracted from an egg shell by wet precipitation method

Abrham Haile

A Thesis Submitted to
The department of Material Science and Engineering

School of Mechanical, Chemical and Materials Engineering
Presented in Partial Fulfillment of the Requirement for the Degree of Master's in Materials Science and Engineering

Office of Graduate Studies
Adama Science and Technology University

Adama
June, 2018

Synthesis and characterization of zinc substituted Hydroxyapatite extracted from an egg shell by wet precipitation method

Abrham Haile

Prof. Sunuk Kim

Dr.Rajalakshmanan Eswaramoorthy

A Thesis Submitted to
The department of Material Science and Engineering

School of Mechanical, Chemical and Materials Engineering
Presented in Partial Fulfillment of the Requirement for the Degree of Master's in Material Science and Engineering

Office of Graduate Studies
Adama Science and Technology University

Adama
June, 2018

Supervisor's/Advisor's approval sheet

To:.....department

Subject: Thesis Submission

This is to certify that the thesis entitled "----------

---------- submitted in partial fulfillment of the requirements for the degree of Masters in ----------, the Graduate program of the department of ----------

and has been carried out by ----------

Id. No ----------, under my/our supervision. Therefore, I recommend that the student has fulfilled the requirements and hence hereby he/she can submit the thesis/dissertation to the department.

_____	_____	_____
Name of major Advisor/supervisor	Signature	Date

Declaration

I hereby declare that this Msc thesis is my original work and has not been presented for a degree in any other university, and all sources of materials used for this thesis have been duly acknowledged

Name: _____

Signature: _____

This Msc Thesis has been submitted for examination with my approval as thesis advisor

Name: _____

Signature: _____

Date of Submission: _____

ACKNOWLEDGEMENT

There are many people without whom this thesis would not have been possible, first and most my family, thank you for all your love, support and encouragement. I wouldn't be here without you by my side

I would like to specially thank my supervisor, Prof. Sunuk KIM, for his support and guidance as a supervisor throughout my project and beyond. I hope we can have same kind of cooperation in the future.

I would like to thank my Co-Advisor Dr.Rajalakshmanan Eswaramoorthy, for his support guidance on this project.

I would like to thank Head of Department of Materials Science and Engineering, Dr. Dinsefa Andoshe, for his support and facilitating all the necessary equipment's, and also working space in the department in addition for outside campus enquiries on the thesis work.

I would like to thank my friends here studying MSc with me currently at ASTU. I appreciate all the spiritual and physical support you have given me while working on experiment until the end.

And all the people all the way who were by my side.

Thank you!!!

List of Acronyms and Abbreviations

ATP	A phosphorylated nucleotide
°C	Degree Celsius
Ca	Calcium
Ca 2+	Calcium ion
CaO	Calcium oxide
$CaCO_3$	Calcium Carbonate
Ca $(NO_3)_2$	Calcium Nitrate
Ca/P	Calcium/Phosphate ratio
CaP	Calcium phosphate
$CaHPO_4$	Dicalcium phosphate
CO_2	Carbon Dioxide
DAHP	3-Deoxy-darabinoheptulosonate-7-phosphate
DNA	Deoxyribonucleic acid
DMSO	Dimethyl sulfoxide
DCPD	Dicyclopentadiene
EDS	Energy-dispersive x-ray spectroscopy
$(NH_4)_2HPO_4$	Diammonium hydrogen phosphate
FT-IR	Fourier Transform Infrared Spectroscopy
FWHM	Full width at half maximum
HA	Hydroxyapatite
ICDD	International Centre for Diffraction Data
Klebsiella pneumoniae	(K Pneumoniae)
KBr	Potassium bromide
K_2HPO_4	Dipotassium phosphate

KOH	Potassium hydroxide
S. aureus	Staphylococcus aureus
TCP	Tetracalcium phosphate
TGA	Thermogravimetric Analysis
XRD	X-ray Diffraction
$Zn(NO_3)_2$	Zinc nitrate
Zn2+	Zinc ion
Zn-HA	Zinc substituted hydroxyapatite
ZI	Zone of inhibition

Contents Page

LIST OF TABLES

Table Page

LIST OF FIGURES

Abstract

Hydroxyapatite was synthesized by wet precipitation method, using egg shell as calcium precursor. To enhance the bioactivity and antibacterial property, zinc was substituted to the HA with a ratio of 0.3, 0.6, 0.9 and 1.2 mol percent. The final precipitate were analyzed by XRD, FTIR, TGA and Disc diffusion method. The XRD data show that for the pure HA and zinc substituted HA in all ratio, pure phase of hydroxyapatite were formed. As the zinc ratio increased however, the lattice parameters, a and c, tend to decrease. In addition, crystal size also show a decrease from 14.3nm to 10.9nm for Pure HA and Z1.2HA respectively. This was in agreement to the FTIR output of the functional groups, in which the decrease in intensity at wavenumber of 1020-1120 cm^{-1}(v3) is characteristic to phosphate groups implying decrease in crystal size. Hence, it imply that zinc has been incorporated to the HA. The other peak in the IR spectrum proof for presence of apatite phase like at bands 574, 609, 966 and 1020-1120 cm^{-1} representing PO_4^{3-} group and the bands at 630 and 3570 cm^{-1} representing of OH group. The thermal analysis indicates the decomposition temperature, that is conversion of hydroxyapatite to TCP (Tetracalcium phosphate) was at 733 ^oC, it is recommended that the heat treatment temperature be set from 450-500^oC. The antibacterial test for one gram positive and one gram negative bacteria, that are S aureus and K Pneumoniae, respectively after 24 hr incubation, show that as the zinc concentration in the apatite increase so as the zone inhibition, giving highest antibacterial activity at Zinc 1.2% substituted HA for both bacteria types. Therefore zinc substituted with 1.2 mol % can be chosen as better HA material for biomedical application considering its satisfactory phase characteristic and its higher antibacterial activity.

Keywords: Hydroxyapatite (HA), Eggshell, Ionic Substitution, Antibacterial Property

CHAPTER ONE

INTRODUCTION

The class of ceramics used for repairing damaged parts of musculoskeletal systems are termed bioceramics. They range in biocompatibility from ceramic oxides, which are inert in the body, to the other extreme of bioresorbable materials. The most widely-used bioresorbable ceramics include calcium orthophosphates (CaPs). They are present in bones, teeth, deer antlers and the tendons of mammals, giving these organs hardness and stability. There are eleven known non-ion-substituted calcium orthophosphates with a Ca/P molar ratio between 0.5 and 2.0 [1, 2]. They are the most sought after biomaterials for the reconstruction of various bone defects especially in the field of dentistry, orthopedic and trauma surgery [3–4]. Due to exceptional biocompatibility [5, 6], osteoconductivity [7], and osteointegration [8], CP-based materials have been under intense investigation for over half a century. The most widely used member of the family of CaPs is hydroxyapatite (HA).

Hydroxyapatite (HA) is an important synthetic biomaterial which is under considerable investigation for many decades due to its similarity with the mammalian hard tissue. Bone and teeth of mammals are composed of Ca (24 wt%), P (10 wt%), proteins (22 wt%), and trace amount of elements like Na^{+}, Zn^{+2}, Mg^{+2}, K^{+}, Si^{-2}, Ba^{-2}, F^{-}, CO_3^{2-}, etc. These trace elements play a crucial role in the life cycle of hard tissue; therefore, scientists are looking at various ways to incorporate the beneficial ions into the structure of synthetic HA to impart it with better osteoconductive [9, 10, and 11] properties. However, a complete match with the mineral components of mammalian hard tissue still remains a challenge. To achieve maximum similarity with the mineral component of bone, biological resources like eggshells, seashells, animal bones, and plants are under extensive investigation to synthesize biological-like HA for various biomedical applications.

Due to the growing importance of HA as a biomaterial, continuous attempts are being made to enhance the biological properties of HA. Although HA crystals are frequently used in orthopedic field, its high dissolution rate in the physiological atmosphere limits its applications in the medical field. Research has shown that the dissolution rates of HA can be altered by incorporating biocompatible ions into its ion-friendly crystal structure [12, 13].

Zn substitution in HA has been the focus of particular interest because of its presence in all biological tissues and its diverse roles in biological functions, such as enzyme activity, nucleic acid metabolism, maintenance of membrane structure and function, hormonal activity, as well as biomineralization [14] and potentially pathological calcification [15, 16]. The uptake and release of Zn in the body are strongly mediated by the bone reservoir, even though it only contains a small portion of the total body Zn [17]. Teeth have also been found to contain a significant amount of Zn, which has been used as an indicator of environmental exposure [18]. It has been recently demonstrated that Zn incorporation into implants may promote bone formation around the material [19, 20].

Hydroxyapatite can either be synthesized from the inorganic components or from the natural organic based materials. Hydroxyapatite prepared from natural bone ash, eggshells, or sea shells can exhibit better biological properties due to the presence of beneficial cations like Na^{+}, K^{+}, Mg^{2+}, Sr^{2+}, Zn^{2+}, and Al^{3+}, or anions like F^{-}, Cl^{-}, SO_4^{2-}, and CO_3^{2-} or the presence of both is proven to be better for different medical applications especially for rapid bone regeneration [21]. The presence of Na^{+} and Mg^{2+} ions play a vital role in the development of bone and teeth, while their absence can cause bone loss and fragility. A simple classification of biological resources for the extraction of HA and its precursors is depicted in Figure 1-1.

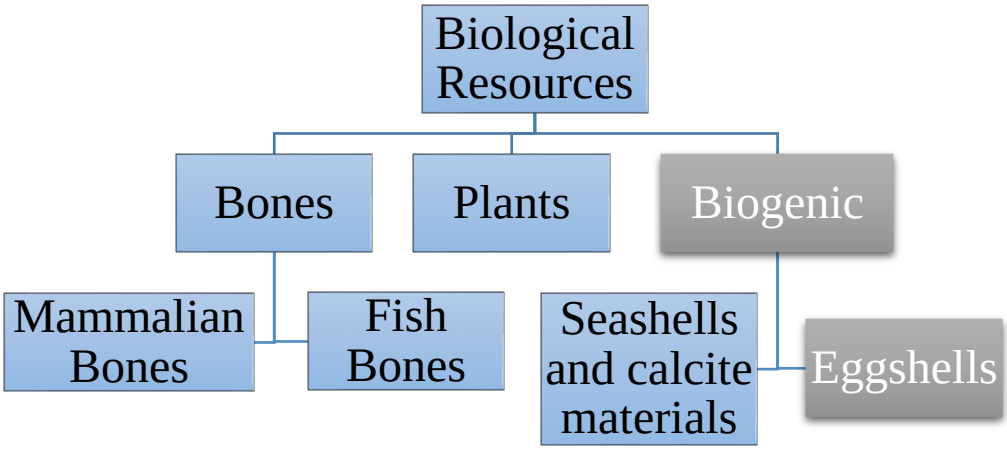

Figure 1-1: Classification of natural resources for the extraction of HA and its precursors [22].

The major problem associated with biomaterials synthesized from the inorganic Ca and P based sources is the high cost associated with the synthetic process [22].

Statement of the problem: -

HA, produced through the conventional way can be used as bone repair and implant coating, however desired efficiency cannot be achieved due to lower bioactivity, no antibacterial property and costly precursors of HA. Therefore using organic egg shell as precursor and zinc as ionic substitute could significantly overcome the limitation of HA mentioned above. And generally can be input for waste material (egg shell) recycling for better environment.

Objective of the research

General Objective**: -** To synthesis pure phase zinc substituted hydroxyapatite extracted from natural waste product that is chicken egg shell.

Specific Objective

- Extract calcium precursor from egg shell to make pure HA and Zinc substituted HA with different ratio
- Characterize Phase, Thermal Stability and microbial property of Pure HA and zinc substituted HA by, XRD, FTIR, TGA and Disc diffusion method
- Compare the properties of Pure HA and zinc Substituted HA

Scope of the study

Synthesis of Hydroxyapatite by wet precipitation method using calcium precursor egg shell, and zinc substituted hydroxyapatite. And characterize them using XRD, FTIR, TGA. Disc diffusion method.

Significance of the study:-

- It contributes for Hydroxyapatite manufacturers an alternative method
- This research can be an input for orthopedic surgeons in Ethiopia
- This method can decrease the production cost of Hydroxyapatite

- The antibacterial property enhancement is going to increase the efficiency of the implant surgery

In this study, it's planned to synthesis Hydroxyapatite by wet precipitation method. The calcium precursor will be from natural waste product that is chicken egg shell. And as many literatures confirmed that zinc improves biological property of the HA in addition to the antibacterial effect, zinc will be incorporated to the HA in the middle of the precipitation synthesis technique. Finally the pure naturally extracted HA synthesized, and the zinc substituted HA extracted from natural waste product will be compared each other and literature

CHAPTER TWO

LITERATURE REVIEW

2.1 Background

Biomaterials

The most accepted definition of biomaterials is, currently the one employed by the *American National Institute of Health* that describes biomaterial as ‘‘any substance or combination of substances, other than drugs, synthetic or natural in origin, which can be used for any period of time, which augments or replaces partially or totally any tissue, organ or function of the body, in order to maintain or improve the quality of life of the individual’’[24].

The first biomaterials used were gold and ivory for replacements of cranial defects. This was done by Egyptians and Romans. Biological materials such as placenta was used since the 1900s. Celluloid was the first man-made plastic used for cranial defects a polymethyl methacrylate (PMMA) was one of the first polymers accepted since World War II [24].

The Williams Dictionary of Biomaterials defined biocompatibility as ‘‘ability of a material to perform with an appropriate host response in a specific situation’’. Although this definition seems vague and unhelpful at first glance, it represented a quantum leap forward at the time of its introduction. Prior to this definition, the prevailing view was that successful materials played largely inert roles the body. A long list of ‘non-properties’ had evolved for ‘successful’ biomaterials: nontoxic, non-immunogenic, non-thrombogenic, non-carcinogenic, and so forth. The above definition required that materials not only provide some function, but also recognized that the interface created by introduction of the material will elicit a biological response. Thus, the idea that the material could be truly inert was essentially rejected with the adoption of this definition. Given today’s level of understanding of our bodies as sophisticated, complex biological environments, the idea that one could place a foreign material without some sort of response seems naïve [24].

Based on the reaction of the tissue to the biomaterial, these are classified into three distinct categories [24]:

1. Bio-tolerant Materials: which are separated from bone tissue by a layer of fibrous tissue.
2. Bioactive materials: which have the property of establishing chemical bonds with bone tissue, known as osseointegration. The collagen and mineral phase of the adjacent bone is deposited directly on the implant surface.
3. Bio-inert Materials: in this class it is possible, under certain conditions, to have direct contact with the adjacent bone tissue. No chemical reactions shall occur between the implant and the tissue.

Ceramic materials for orthopaedic applications were introduced in the 1970s, where failures of the biomaterials in use then, such as steel, cobalt alloys and poly (methyl methacrylate), began to be detected. Hence, attention was directed to ceramic materials in an attempt to find good bone integration features.

Hydroxyapatite, (HA), and other related calcium phosphate minerals are used extensively to improve the integration of femoral implants into the hip joint. HA appears the most promising due to its outstanding biological properties such us atoxicity, lack of inflammatory response and absence of fibrous or immunological reactions [25]. HA possesses identical chemical composition and high biocompatibility with natural bone [26].

Bioactivity is related to a modification of the surface of the material with formation of naturally induced; biologically equivalent HA as a result of dissolution, precipitation and ion exchange reactions with the physiological environment. This ability to bond to bone tissue without the formation of a fibrous tissue layer at the bone - implant interface is extremely important since it guarantees the fixation and stabilization of implants and prostheses. The bone - implant interface mimics the type of interface that is formed when natural tissues repair themselves; it is dynamic in its nature, changes with time and requires a controlled degree of chemical reactivity of the ceramic [26]. Hence, the clinical advantage of HA is due to its bioactive characteristics, which is dependent upon its synthetic structure such as chemical stoichiometry, crystallinity and surface morphology [25]. HA has many crystallographic features that are

similar to those of natural bone tissue; although they show insufficient mechanical reliability for medical applications where high loads are required [25].

Several attempts to determine the exact composition of HA via chemical analysis were undertaken in the first half of the 18th century. About a century later, the current concepts of synthesizing materials comprising of the various calcium phosphate crystal phases was introduced [27]. Most calcium phosphates are classified as resorbable biomaterials. This means that under physiological conditions they will dissolve. The benefit of calcium phosphate biomaterials is that the dissolution products can be readily assimilated by the human body.

The following sections will discuss literatures regarding, human bone composition, the various methods of synthesizing HA will also be considered. Then substituted hydroxyapatite and extracting HA from natural wastes will be covered. At the end product of synthetic bone produced from, that is, HA, will then be analyzed on account of the attainable physical properties, and antibacterial properties.

2.2 Biological apatite

2.2.1 Natural Human Bone Mineral

Basic knowledge of the physical, chemical, and mechanical properties of natural human bone is critical for the development of bone-like materials. The study of biological apatite (that is, human bone mineral) has been widely investigated. As a result, their chemical composition and structure is well understood. Natural human bone has a varied arrangement of material structures at many length scales which work in harmony to perform diverse mechanical, biological and chemical functions; such as structural support, protection and storage of healing cells, and mineral ion homeostasis. Scale is of importance in discussing bone architecture as the structure is hierarchical and complex. In order to understand the mechanical properties of bone material, it is important to understand the structural relationship between them at the various levels of hierarchical structural organization This section therefore, outlines the various levels associated with the hierarchical structure of human bone, the chemical composition for the biological apatite mineral (carbonated apatite), the physiology of bone, bone remodeling, and biological responses.

2.2.2 Hierarchical Structure of Bone

Despite the variety of external forms, the internal structure of bone is relatively consistent. Bone structure is hierarchically organized, which means that bone displays different structural entities at different length scales [28, 29]. Four structural levels of hierarchy can be distinguished in adult human bone. These levels will be denoted as the continuum level (or level 0), tissue level (level 1), cellular level (level 2) and molecular level (level 3). The structural entities at each level will be denoted as the macrostructure, mesostructure, microstructure and nanostructure, respectively. The hierarchical structural organization in human bone is summarized in Figure 2-1 below.

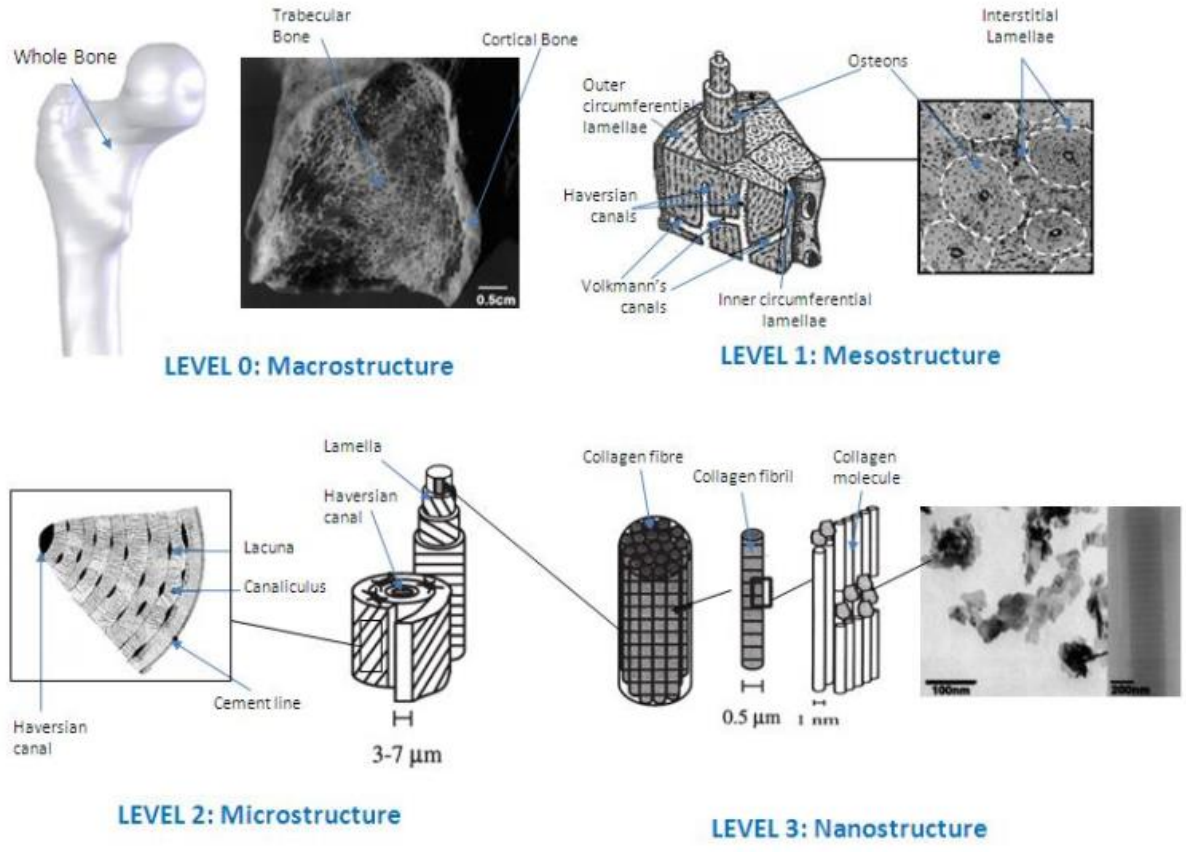

Figure 2-1: Hierarchical structural organization of bone: Level 1: cortical and cancellous bone; Level 2: osteons with Haversian systems and lamellae; Level 3: collagen fiber assemblies of collagen fibrils and Level 4: bone mineral crystals, collagen molecules, and non-collagenous proteins. Adapted from [28, 29, 31].

2.2.3 Macrostructure

At the continuum level, the scale of 5 mm and higher, the bone structure is classified according to its porosity. The two classifications are cortical (or compact) bone and trabecular (or cancellous) bone. Cortical bone has a porosity ranging between 5% and 10%, and it is usually found along the exterior shaft section of long bones. Cortical bone forms the outer shell around the trabecular bone in joints and in vertebrae [32]. Trabecular bone has a porosity ranging from 75% to 95%. It is usually found in cubicoidal bones (such as, vertebrae), flat bones (such as, the pelvis) and the end of long bones (such as, the femur). The non-mineralized spaces within trabecular bone contain bone marrow, which is a tissue composed of blood vessels, nerves and various types of cells. Cortical bone accounts for about 80% of the total skeletal mass while trabecular bone constitutes some 70% of the skeletal volume. The anisotropic structure of bone leads to mechanical properties that exhibit directionality. This directionality results from the fact that bone has evolved to be both tough and stiff, two competing properties which are optimized in bone but with an inherent loss in isotropy. Nevertheless, bone exhibits extraordinary mechanical properties, displaying both viscoelastic and semi-brittle behavior. The microstructure produced by the compaction of cancellous bone is composed of irregular, sinuous convolutions of lamellae. In contrast, the microstructure of cortical bone is composed of regular, cylindrically shaped lamellae. Therefore, reliable differentiation can only be achieved by microscopy methods.

2.2.4 Mesotructure

At the tissue level, the scale of 100 μm to 1 mm, major differences can be identified within the cortical and trabecular structures. Cortical bone is composed of osteons or Haversian systems. The osteons (150 to 300 μm in diameter and up to 3 to 5 mm in length) are embedded in a matrix of lamellar bone known as interstitial lamellae [30]. The central cavity inside an osteon is known as the Haversian canal. Haversian canals are typically 40 to 50 μm in diameter and run along the long axis of a bone. Normally a blood vessel (15 μm in diameter) as well as nerve terminations are found inside Haversian canals. Volkmann‘s canals are short transverse channels connecting the Haversian canals. These canals also contain blood vessels and probably nerves [32]. The mesostructure of trabecular bone is composed of plates and struts called trabeculae. Sometimes trabeculae appear organized into orthogonal

arrays, but they are often more randomly arranged. Each trabecula is about 200 μm thick. Rarely, it is possible to find trabeculae thick enough to contain a blood vessel and some osteon-like structure. Within a trabecula, one can find trabecular packets, which are the product of new tissue formed after remodeling. A typical trabecular packet is about 50 μm thick and 1 mm long.

2.2.5 Microstructure

At the cellular level, the scale of 5 to 50 μm, two types of bone can be found: woven bone and lamellar bone. Woven bone is a poorly organized tissue and may usually be found in adults post fracture injury. With maturation, the woven bone is converted into lamellar bone. Lamellar bone, adversely, is a slowly formed, highly organized bone tissue consisting of lamellae. The lamellae are bands or layers, 3 to 7 μm thick, forming an anisotropic matrix of mineral crystals and collagen fibers. Woven bone may become more highly mineralized than lamellar bone, which may help to compensate for its lack of organization [32]. Trabecular packets and osteons are formed of lamellae and attached to the bone matrix by cement lines. The cement lines are found where bone resorption ends and bone formation begins. They are about 1 to 5 μm in thickness. The ―porosities‖ at this level are identified as lacunae (ellipsoidal holes) and canaliculi (micro-channels) (refer to Figure 2-1). Canaliculi are about 0.2 μm in diameter [33].

2.2.6 Nanostructure

At the molecular level, the scale of 100 nm and smaller, there exists three main materials of importance, such as biologic apatite crystals, collagens, and noncollagenous organic proteins. The mature crystals are not needle-shaped, but plate-shaped [28, 30]. Plate-like biological apatite crystals of bone occur within the discrete spaces within the collagen fibrils, thereby limiting the possible primary growth of the mineral crystals, and forcing the crystals to be discrete and discontinuous. The mineral crystals grow with a specific crystalline orientation—the *c* axes of the crystals are roughly parallel to the long axes of the collagen fibrils [28, 30]. The average lengths and widths of the plates are 50 x 25 nm. Crystal thickness is 2–3 nm [28, 30]. The Nano-crystalline bone apatite has small but significant amounts of impurities such as HPO_4, Na, Mg, citrate, carbonate and K [30]. The carbonate apatite crystal, not only exhibit a hexagonal crystal structure but is shown to produce x-ray diffraction

patterns, analogous to that of HA [28]. An explanation for their plate-like structure is proposed by Weiner et al. [28] in that they grow via an octacalcium phosphate transition phase. Octacalcium phosphate crystals are plate-shaped and have a structure very similar to apatite, except for the presence of a hydrated layer.

2.2.7 Chemical Composition of Human Bone Mineral

Natural bone can be considered to comprise of both organic and inorganic material. Moreover, 90 – 95% of the organic component consists of collagen whilst the inorganic component consists primarily of calcium and phosphate [34, 35].

A typical wet cortical bone is composed of 25 wt. % organic phase (that is, the matrix), 62 wt. % inorganic phase (that is, carbonated apatite; HA), 10 wt. % water and 3wt. % residual (See Figure 2-2). The organic phase consisting mainly of collagen laid down in the form of fibers aid in the provision of flexibility to bone. As discussed previously, the inorganic phase consists of submicroscopic crystals of an apatite of calcium and phosphate, whose crystal structure resembles that of carbonate HA and other mineralized phases, such as, chlorapatite (ClAp), fluorapatite (FAp), sodium-containing apatite and magnesium-containing apatite. The mineral phase is made of a continuous cellular structure, which gives good mechanical strength. HAp is the main mineral constituent for bone, dentin and teeth. [34, 35]

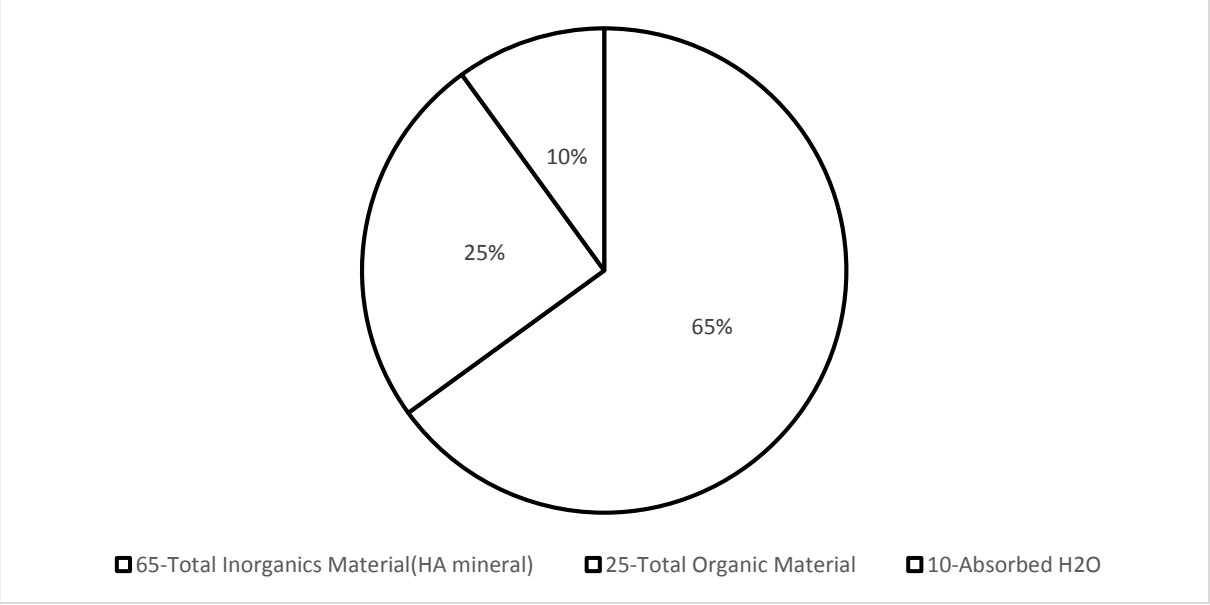

Figure 2-2: Chemical compositional analysis of human bone [34, 35]

As an estimate per weight, bone tissue is composed of 25% water, 43% mineral, 29% collagen and 3% of non-collagenous organic molecules (refer to Figure 2-3) [32]. Bone stores 99% of the total body calcium while the remaining 1% circulates in the blood [30].

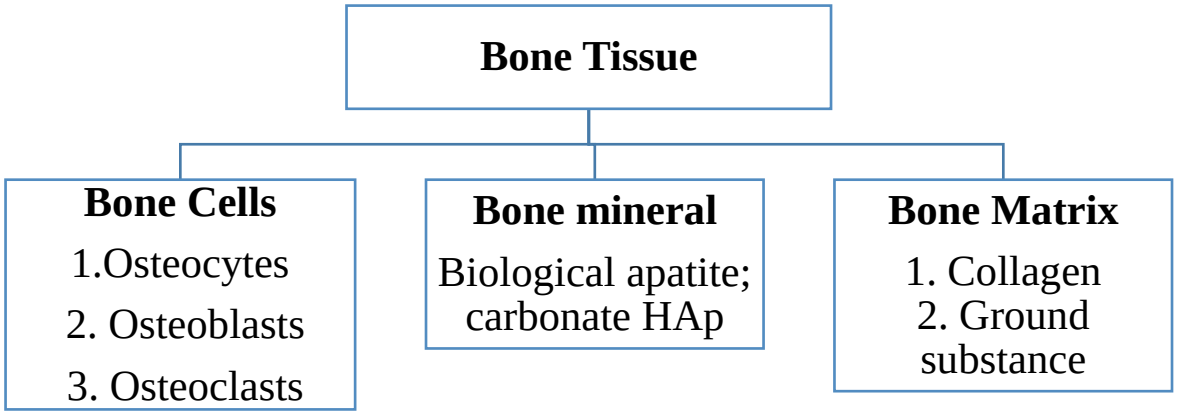

Figure 2-3: Comportments of human bone tissue [32].

The inorganic component of human bone consists of calcium compound, as identical to synthetic carbonated HA, made up of calcium ions, phosphate ions and hydroxyl ions in the ratio of the chemical formula, $Ca_{10}(PO_4)_6(OH)_2$. The constituent elements within bone mineral are given in Table 2-1. Mg, Na, K and carbonate ions are also present in bone salts, although they are not organized into specific crystals. Fluid Ca-P compounds in the matrix are transformed to HA.

Table 2-1: Composition of the mineral phase in human bone. Adapted from [34-35].

Mineral Component Constituents (wt. %)	Chemical formula	Enamel	Bone
Calcium	Ca^{2+}	36.0	24.5
Phosphorous	P	17.7	11.5
Ca/P molar ratio		1.62	1.65
Carbonate	CO_3^{2-}	3.2	5.8
Sodium	Na^{+}	0.5	0.7
Magnesium	Mg^{2+}	0.44	0.55
Potassium	K^{+}	0.08	0.03
Chloride	Cl^{-}	0.30	0.10
Floride	F^{-}	0.01	0.02
Total inorganic mineral		97.0	65.0
Total organic absorbed H_2O		1.0	25.0
Trace Elements	Sr^{2+}, Pb^{2+}, Zn^{2+}, Cu^{2+}, Fe^{3+}	1.5	9.7

While the main mineral components forming human bone are calcium (36.7 wt. %) and phosphorous (16.0 wt. %) with trace amounts of other minerals [38]; a significant amount of carbonate (7.4 wt. %), also appears to be present within the biological apatite, bone. Slosarczyk et al. [37] confirm that biological apatites present in; bone; dentin and enamel contain different amounts of carbonate 7.4: 5.6: 3.5 wt%, respectively. The presence of CO_3^{2-} in their structure is of paramount importance; as itis the main source of lattice distortion, creating micro-stresses and crystalline defects in its vicinity which, in turn, play a fundamental role in its solubility. As a consequence, synthetic apatites aimed at emulating the biological scenario should exhibit small particle sizes and the presence of CO_3^{2-}[25]. The apatite crystals which form natural bone are smaller than 500 Å (nm) in size. This is a critical factor in

understanding the solubility of biological apatites and the continuous bone regeneration due to constant dissolution–crystallization cycles [25].

2.3 Synthetic apatite

2.3.1 Hydroxyapatite (HA) Calcium Phosphate

Calcium phosphate in the form of crystallized HA and/or amorphous calcium phosphate (ACP) provides stiffness to the bone [39]. The mechanical properties of natural human bone depend largely on the humidity of its surrounding environment [38]. HA ceramics do not exhibit any cytotoxic (cell-killing) effects; rather it shows excellent biocompatibility with hard tissues and also with skin and muscle tissues. Moreover, HA can bond directly to bone [26, 34, 35, and 39]. The benefits of HA materials in coated implants have been widely acknowledged, but the occurrence of several poor performances such as improper melting of the feedstock after spraying, reproducibility and satisfying biomedical requirements has generated concerns over the consistency and reliability of thermally sprayed HA coatings [40]. Recent investigations using HA coatings have shown that process related variability has a significant influence on coating characteristics such as phase composition, structure and chemical composition, and performance such as bioresorption, degradation and bone apposition [26]. Variation in process parameters such as powder morphology can induce microstructural and mechanical inconsistencies that have an effect on the service performance of the coating [40, 41].

Ca/P ratios from 1.5 - 2.0, of HA, are commonly used for orthopaedic applications in the form of bioceramic coatings [25]. The ideal Ca/P ratio for stoichiometric (that is, pure, single phase) HA is 1.667 and the theoretical density is 3.156g cm^{-3} [34, 35, 42]. However, Suchanek et al. [43] reports that the Ca/P ratio does not significantly influence the grain growth of the HA ceramics. Many studies conducted around the synthesis of HA, show that a pH > 9.0 provides an appropriate environment for the formation of stoichiometric pure HA powders [26]. HA is the most stable calcium phosphate salt at physiological temperatures.

2.4 Techniques for preparing synthetic HA

The various methodologies employed to produce synthetic HA are discussed in this section to provide the necessary background information with respect to HA powder production techniques, used to date. The production of synthetic ceramic HA powders may be classified under four main headings [44]:

a. Wet Chemical Synthesis (such as, Precipitation, Hydrothermal, Hydrolysis and Sol-Gel Techniques)
b. Dry Chemical Synthesis (such as, solid-state reactions, mechano-chemical synthesis)
c. Vapor Phase Reactions (such as, spray and freeze-drying)
d. Novel Techniques

Since the present research utilizes the wet chemical precipitation method to synthesize phase pure HA, this method is discussed in detail, with an overview of other possible synthetic routes for its synthesis.

The main advantage associated to the wet process, is that its by-product consists primarily of water and the probability of contamination during processing is very low. Low processing costs has also been reported. Its disadvantage is that the resulting product can be greatly affected by even a slight difference in the reaction conditions. The dry process, on the other hand shows high reproducibility in spite of the high risk of contamination during stages of milling and long heat treatment times [26, 35, and 45].

2.4.1 Chemical Precipitation Route

In the precipitation route, HA powders are obtained from a chemical reaction of inorganic oxide solutions [42]. The two most popular ways in precipitating HA are described in the two reactions below [26, 42, and 46]:

A. Reaction 1

The precipitation method for the reaction of orthophosphoric acid with calcium hydroxide:

$$10Ca(OH)_2 + 6H_3PO_4 \rightarrow Ca_{10}(PO_4)_6(OH)_2 + 18H_2O \qquad (2-1)$$

B. Reaction 2

The precipitation method for the reaction of diammonium hydrogen phosphate with calcium nitrate:

$$10Ca(NO_3)_2 + 6(NH_4)_2HPO_4 + 8NH_4OH \rightarrow Ca_{10}(PO_4)_6(OH)_2 + 20NH_4NO_3 + 6H_2O \quad (2-2)$$

Reaction 1 is simple, cheap, suitable for large scale industrial production and nonpolluting by nature, but often leads to the production of non-stoichiometric HA, which creates subsequent problems during sintering (thermal decomposition of nonstoichiometric HA leads to TCP when the Ca/P molar ratio < 1.67), or to CaO when the Ca/P molar ratio > 1.67. In contrast, Reaction 2 is expensive to produce and polluting by nature, in that it‘s by products must be removed.

HA synthesized using Reaction 2, have found that the reaction temperature, the reactant concentrations, rate of mixing the reactants and the residence time can affect the overall characteristics of the HA produced [26].

HA with a Ca/P molar ratio, ranging from 1.5 to 1.667 ($0 \leq x \leq 1$) using the conventional aqueous precipitation method from the addition of a diammonium phosphate solution ($(NH_4)_2HPO_4$) into a reactor containing a calcium nitrate solution was prepared can be prepared. [41]. The device implemented was fully automated with the reactor placed in an argon atmosphere under dynamic flow in order to prevent any presence of CO_2, which could result in carbonate apatite formation. In this study, pH and temperature of synthesis were the preponderant parameters for the control of the precipitate composition

Overall, precipitation techniques can produce small particle size and high-purity HA powders, when the precipitation system and conditions are well controlled to obtain a reproducible precipitate. The important precipitation process variables include solution concentration (Ca/P ratio), pH, acid addition rate, stirrer speed, temperature, reaction time and atmospheric condition. [26]

2.5 Substitution in synthetic HA

Ionic substitution in apatites can be well illustrated in geological apatites. The geological environment provides a wide range of elements, and temperatures can reach hundreds of degrees Celsius, which makes the apatite structure more prone to substitutions, e.g. OH, Cl and F anions can substitute for each other in the channel sites in almost any proportion. Anionic complexes can replace the phosphate group and a large number of bivalent and trivalent metal cations can substitute for calcium. In fact, apatite is able to incorporate almost half of the elements of the periodic system in its atomic structure [48]. However, laboratory conditions related to temperature and pressure do not enable such a wide range of options as are enabled by a geological environment, in synthetic hydroxyapatite substitutions. The incorporation of ions into the HA structure will result in some structural changes, which can be detected with various analytical techniques. Ionic substitution can affect the crystal structure, the crystallinity, the surface charge, the solubility and other vital properties, leading to major changes in biological performance upon implantation.

Some previous studies on synthetic hydroxyapatites have explained the role of substitution of biocompatible cations, such as Mg^{2+}, Zn^{2+}, and $Sr2^{+}$. Substitutions of bivalent ions can cause no charge imbalance in the apatite lattice, but substituted monovalent ions like Na^{+} and K^{+} cause a charge imbalance that can be neutralized by creating supplementary vacancies [49], or by the occurrence of simultaneous substitutions of cations and anions without the formation of any vacancy or loss of charge balance [50].

Replacement of Ca^{2+} ions by other cations can lead to contraction or expansion of the lattice parameters, depending upon ionic size. It might be assumed that more voluminous cations can modify the cell volume and also extend the a-axis parameter. However, this statement is not valid, mainly in cases when a bivalent cation is substituted by a monovalent cation. The formation of vacancies in the channel reduces the diameter of the channel diameter, and consequently reduces the parameter [51].

The localization of substituting cations in the apatitic structure is also generally correlated to their ionic radius [52]. Site Ca (I) is smaller in volume than site Ca (II) [53]. Simplistic reasoning might lead to the conclusion that a cation with a larger radius than radius of Ca^{2+} must prefer and occupy site (II). However, some experiments have shown the converse. The

kind of anion in the channel is probably of great importance. As an example, in fluorapatite, the Mn^{2+} ion (0.080 nm) substitutes for calcium (0.099 nm) in site (I); however, in chlorapatite, it substitutes simultaneously in both sites [52].

The charge of the ions and the strength of the corresponding bonds affect the distribution of the cations between these two sites. Another explanation is that the driving force in the distribution process is optimization of the Metal–Oxygen interaction: site (I) allows larger cations to be accommodated because of the longer Metal (I)–O distances. However, when the number of the bigger ions increases, the repulsion between atoms in the Metal (I) position would cause an enlargement of the c-axis, which is partially restrained by accommodating metal atoms in site (II) [54]. To maintain the charge balance, trivalent cations would be incorporated as lower valence hydroxo-ions. The ion exchange ability of trivalent ions seems to depend more on their charge density than on their ionic radii [55]. Monovalent anions (F, Cl) substitute OH anions in the anion channel without charge imbalance. Bivalent anion (HPO_4^{-2}, CO_3^{-2}, SO_4^{-2}, SeO_3^{-2}, SeO_4^{-2}) substitutions instead of the trivalent phosphate group are balanced by the formation of both hydroxide and calcium vacancies.

In the case of tetravalent anion (SiO_4^{-4}) substitutions, the negative charge are compensated by a hydroxide vacancies. Synthetic HA is not ideal for use as a bone substitute in loadbearing applications, due to its brittleness and lack of strength. Other disadvantages include a high degree of crystallinity, which results in reduced degradability of pure HA when it is implanted into the organ. In order to overcome this obstacle, HA is doped or substituted with various metals, such as magnesium [56–58], manganese [59], zinc [60], titanium [61] and strontium [47] to improve its mechanical strength. Moreover, minerals and traces of metal elements accelerate bone formation [54] and resorption on bone cells or bone mineral in vivo and in vitro [47].

2.5.1 Cationic substitution - Zinc

Incorporation of zinc into the HA structure (Zn-HA) has been abundantly studied, owing to the key effect of Zn^{2+} cations in several metabolic processes that make zinc eligible for use in many biomedical applications. Zn-HA has been prepared predominantly by a precipitation method [62–68], but ion-exchange [89], a hydrothermal technique at 200 ^{o}C [60] and the sol–gel process

[70] have also been used. Precipitation processes have been implemented at room temperature [62, 63, 66, and 68] or in the temperature range of 60–90 ^{o}C [64, 65, 67, and 71].

The crystallinity and the substitution content of Zn in Zn-HA prepared with a NaOH solution was higher than the crystallinity and the substitution content of Zn in Zn-HA prepared by an ammonium aqueous solution [60]. Systematic studies of incorporation and co-precipitation [67, 68] have shown that considerable amounts of Zn can be incorporated into HA.

Progressive Zn substitution in HA, and their findings indicate that with increasing Zn concentration the final product changes from Zn substituted apatite to an amorphous apatite-like phase [67]. It's suggested that the substitution limit of Zn in HA is 15 mol% [67], unlike some suggesting it can go up to 25 mol% [68].

The inhibiting effect of zinc on HA crystallization and its preference for a β-TCP structure closely resembles the behavior previously observed for magnesium [69, 72]. The lattice parameters of Zn-HA changed owing to the difference in ionic radius between Zn^{2+} (0.074 nm) and Ca^{2+} (0.099 nm). The C lattice parameter of Zn-HA was found to decrease progressively with increasing Zn concentration [67]. They also observed an increase in the a-lattice parameter for a higher Zn concentration (5 mol%). This was ascribed to increased H_2O substitution for OH. Studies [60, 71, 73] have observed a decrease in lattice parameter a, with a Zn fraction up to 10 mol% Zn, and then the parameter begins to increase. Lattice parameter c decreases monotonously as the Zn fraction increases. Some researchers have systematically examined the local structure of Zn incorporated into HA at low concentrations by combining experimental and spectroscopic results with density functional theory calculations [65]. These calculations unequivocally showed that substitution in the Ca (II) position is more energetically favored. Which employed an embedded cluster LCAO (linear combination of atomic orbitals) method [74-77].

Additionally Ca (II) site is to be favored for Zn substitution at the HA (0001) surface. Hence its suggested that Zn is octahedrally coordinated [74 and 78] (Fig. 2-4 (A)), but the some calculations showed that the most favorable structure for Zn is tetrahedral coordination, as shown in Fig. 2-4 (B) [65 and 75],

Looking more closely at tetrahedral coordination (Fig. 2-4 (B)), it can be seen that among the four oxygen atoms bonded to Zn, one is from the nearest hydroxyl group and three are from the adjacent phosphate groups. This arrangement of the atoms causes a reduction in the a-lattice parameter from 0.9488 to 0.9319 nm. The hydroxyl group moves off its c-axis position and the Zn atom moves off the Ca(II) site. Both come close to each other,

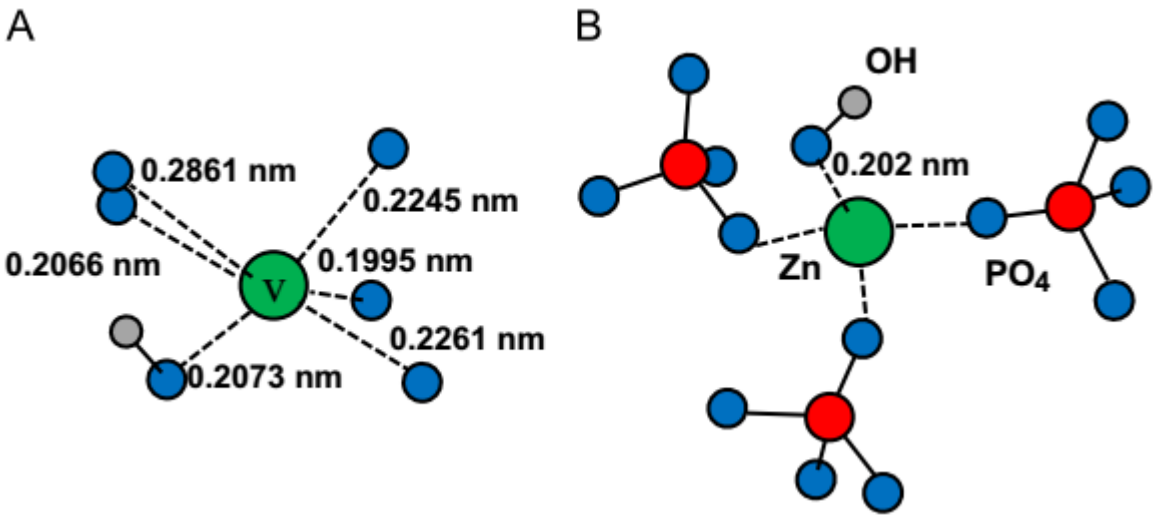

Figure 2-4: Detailed view of the local coordination of Zn incorporated in the HA structure with interatomic distances. (A) Octahedral coordination, suggested by Terra et al. [74] and by Ma and Ellis [78]; (B) tetrahedral coordination, suggested by Tang et al. [65].

And the Zn–O(OH) distance is 0.202 nm compared to 0.269 nm in ideal distances in HA.The preference of Zn for the Ca (II) site may facilitate the uptake and release of Zn by bioapatite because it would not disrupt the framework of the structure.

2.6 Extracting hydroxyapatite and its precursors from Biogenic sources (Egg Shells)

Every year millions of tons of eggshells are thrown as waste material all around the world. A large amount of eggshells is produced as waste from houses, restaurants, hatcheries, and bakeries. Similarly, a huge amount of sea shells and other calcite materials are also present in the universe. An eggshell contains calcium carbonate (94 %), magnesium carbonate (1 %), CP

(1 %), and organic substances (4 %) [80]. Being cheap and easily accessible, eggshells are considered a good source of calcium precursor required for the synthesis of HA.

Traditionally HA is either made dense or porous by sintering it at high temperature where mechanical properties are controlled by controlling the various factors like sintering temperature, duration of sintering, and composition of the ceramic material used. In this regard, sea shells and eggshells are considered the better selection to synthesize good-quality biomaterials as they resemble the human hard tissues. Some Molluscs shells (containing 95–99 % $CaCO_3$) bear better nanoscale regularity, mechanical properties, and compression strength than common mineral crystals [81, 82]. To extract CaO the shells are washed with boiling water or steam to remove the impurities and then the shells are crushed to powder followed by heating at elevated temperature to furnish CaO. This CaO can be reacted with phosphorous precursors to prepare HA according to the following reaction [80].

$$CaCO_3 \rightarrow CO_2 + CaO \qquad 2-3$$

$$3Ca_3(PO_4)_2 + CaO + H_2O \rightarrow Ca_{10}(PO_4)_6(OH)_2 \qquad 2-4$$

Carbonated HA nanoparticles constitute the inorganic part of enamel, teeth, and bones and its concentration ranges a few percent in weight [79, 83]. The incorporation of CO_3^{2-} ions in the apatite structure affects its structure, morphology, and results in better biochemical reactivity of bone minerals [84, 85]. Therefore, CO_3^{2-} substituted HA nanoparticles are considered to be a good candidate for bone and dental applications [86].

Hydroxyapatite and β-TCP uniform in size were successfully synthesized using recycled eggshells and phosphoric acid [87]. Washed uncrushed eggshells were calcined at 900 ^oC to remove organic matter. The calcined eggshells were ball milled with phosphoric acid (1:1.1 ratios) for 24 h followed by calcination at 900 C for 1 h to furnish HA with Ca/P ratio of 1.65. Phase purity of final product depended on the ratio of CaO from eggshells and phosphoric acid used. Calcium carbonate present in the mollusks shells (Pomacea Lineata) was converted into HA powder through in vitro treatment by soaking in phosphate solution at room temperature [88]. SEM analysis showed the formation of flower-like arrangement of interconnected platelets with sponge-like organization. XRD study indicated the formation of HA from aragonite after

7 days of soaking in phosphate solution, while the FTIR analysis confirmed a complete conversion of aragonite to HA after 30 days.

Hydrothermal and thermal calcination methods were used to synthesize HA from natural coral exoskeleton and xenogeneic bone, respectively [89]. XRD analysis confirmed the formation of phase-pure HA as no peaks for other phases such as TCP, CaO, and $CaCO_3$ were observed. However, peak shifting and deviation of lattice parameters from the standard observed for HA extracted from xenogeneic (bovine) bone was attributed to the presence of carbonate ions in the HA structure. Coral pre-treated with sodium hypochlorite was subjected to series of hydrothermal treatments to furnish highly porous Si-incorporated HA [90]. XRD analysis confirmed the formation of phase-pure HA, while EDS studies confirmed the presence of Si and Mg in addition to Ca, P, and O. The presence of Mg in the final product was attributed to the high Mg concentration in seawater. The resulting porous structure with 70 % porosity possessed exceptional compressive strength of 5.5 MPa, a value much higher than the cancellous bone and porous HA structures with similar degree of porosity.

In situ HA synthesis was carried out by reacting crushed and washed eggshells with hydrochloric acid and DAHP solution for one week at room temperature [91]. Eggshells were not calcined to remove organic matter such as amino acids, proteins, and glycoproteins prior to their use. Authors concluded that the presence of these molecules helped to control the shape and size of the nanoparticles. However, the presence of these biomolecules in the final product will hinder its biomedical application due to obvious ethical issues.

Calcium oxide from thoroughly washed and calcined hen eggshells was irradiated in microwave at 800 W in the presence of DAHP to furnish nanosized HA (18 nm) [92]. Increased MG-63 osteoblast cells growth after 1 day confirmed the non-cytotoxic nature of the hen eggshell-derived HA.

Polycrystalline nanosized B-type cHA was synthesized through sol–gel reaction between the calcium source from chicken eggshells and potassium dihydrogen phosphate [93]. XRD analysis confirmed the formation of singlephase HA while TEM studies confirmed the formation of polycrystalline material of prolate spheroidal morphology with average particle size of 35–50 nm.

In another research, HA was synthesized by reacting reagent-grade phosphoric acid with $CaCO_3$ extracted from hen eggshells through a precipitation method followed by heating at 900 ^oC to prepare crystalline powder [94]. XRD and FTIR studies confirmed the formation of HA and the presence of hydroxyl and phosphate groups, respectively, while Ca/P ratio of 1.63 was determined through gravimetric and spectrophotometric analysis. Microwave irradiation of the reaction mixture containing eggshells and DAHP in the presence of EDTA furnished flower-like nanostructures of HA having crystallite size of 78 nm [95]. The presence of peaks at 1415, 1459, and 875 cm^{-1} in FTIR spectra confirmed the formation of B-type substituted cHA, while EDX analysis confirmed the presence of Mg as trace ion. Through precipitation technique nanosized HA was synthesized by employing hen eggshells as calcium source [96]. EDX results showed that the Ca/P ratio proportionally depended on the pH of the reaction mixture. pH of the reaction mixture also influenced the phase composition of HA, where at lower pH value, whitlockite was observed as secondary phase. Ball-milled slurry of crushed oyster shells (Crassostrea gigas) and calcium pyrophosphate in 4:3 ratio was dried in oven at 150 ^oC for 12 h, followed by heat treatment at temperatures between 900 and 1100 ^oC furnished HA with β-TCP and calcite as secondary phases [97]. However, in case of reaction between oyster shell powder and DCPD followed by milling for 5 h and heat treatment at 1000 ^oC, no secondary phase was observed.

At heating temperature of 900 ^oC the product existed in multiple phases mentioned above; however, increase in the heating temperature resulted in the conversion of calcite into β-TCP due to their structural similarities and β-TCP was transformed to HA due to the higher thermodynamic stability of HA than β-TCP when calcination was carried out at 1100 ^oC. Ground waste eggshells were hydrothermally treated with DAHP at 80–160 ^oC for 2 days to furnish multi-phase CPs [98].

Phases like monetite ($CaHPO_4$), whitlockite $Ca_3 (PO_4)_2$, and HA were formed at low heating temperature of 80 ^oC; however, the increase in heating temperature to 160 ^oC resulted in the predominant formation of HA. This increase in heating temperature also influenced the particle morphology, which changed from small particles with the laminar-plate structure at 80 ^oC to scattered flower-like agglomerates and small prisms with smooth surfaces at 140 ^oC followed

by hashed micro-sheets at 160 ^{o}C. Formation of HA nanoparticles from eggshell wastes and fruit waste extracts was reported recently [99].

Biomolecules present in the fruit waste were used to provide nucleation site for HA nuclei; furthermore the biomolecules along with hydrothermal treatment substantially influenced the particle size and morphology. XRD analysis confirmed the formation of poorly crystalline monophase of HA, this low degree of crystallinity was attributed to the presence of A-type and B-type carbonate group in the HA structure. ICP-AES confirmed the presence of Na (0.410 wt%), Mg (0.390 wt%), and Sr (0.289 wt%) in addition to Ca (37.2 wt%) and P (17 wt%), however, it was not clear whether the presence of trace elements was due to the eggshells used or the extract from the pomelo peel. Solid-state reaction between CaO produced from eggshell waste with dicalcium phosphate dehydrate (DCPD) resulted in the formation of HA [100]. The phase purity was dependant on the heating temperature and duration, where higher heating temperature of 1100 ^{o}C for 5 h furnished pure HA. High Ca/P ratio of 2.20 was attributed to the presence of B-type carbonate group, which had substituted the phosphate group. A pyrolysis wet-slurry precipitation method was used to synthesize HA using CaO derived from mussel shells (Perna canaliculus), which are abundantly available in New Zealand [101]. XRD of the as-synthesized HA confirmed the formation of nanosized, crystalline HA with trace amount of calcite, which was removed through calcination at 800 ^{o}C. The presence of carbonate peaks in FTIR spectra was attributed to the adsorbed CO_2 from the atmosphere. EDX spectra of the heat-treated HA confirmed the Ca/P ratio to be 1.66, while the presence of potassium ions was attributed to the inadequate washing of the samples.

Thoroughly washed, cleaned eggshells were reacted with nitric acid to produce calcium nitrate, which was later reacted with phosphoric acid to furnish cHA [102]. Affinity of HA for cations was exploited and the synthesized HA was used for the removal of Pb^{2+} ions from the aqueous solution under acidic conditions. Good affinity of HA toward Pb^{2+} ions was attributed to the adsorption of Pb^{2+} ions on the surface of HA and an ion-exchange process between Ca^{2+} of HA and Pb^{2+} ions in aqueous solution.

Hydrothermal treatment of calcined eggshells and DAHP in mixed solvent system comprising DMF and hydrogen peroxide under acidic conditions at 120 ^{o}C for 24 h resulted in the formation of flower-like cHA structures [103]. XRD results showed well-crystallized 002 plane, while the

broadness of other peaks width indicated partial crystallization of the material. Authors reported that the morphology of particles was strictly dependent on the temperature of hydrothermal treatment and the ratio of the mixed solvent systems.

Biogenic calcite extracted from spines collected from various species of Paracentrotus lividus sea urchins was converted to HA through hydrothermal treatment in the presence of sodium phosphate solution at 180 ^{o}C for 24 h [104]. During this pseudomorphic transformation the calcite crystals of the original spine were replaced by the nanosized elongated apatite nanocrystals, which resulted in the change of density and porosity in the final product. Furthermore the product not only inherited the external morphological features of the sea urchin spines but the complex internal porous structure was also retained.

Micrometer-sized whiskers of HA were successfully synthesized using $CaHPO_4$ and CaO obtained from eggshells through a hydrothermal method at 170 ^{o}C for 48 h [105]. Surface area (50 m2/g) and particle size (0.06 μm) were calculated using BET results and XRD of the resulting calcined powder (700 ^{o}C) confirmed the formation of HA and $CaHPO_4$ in 3:1 ratio. Phase-pure HA was synthesized through a self-assisted chemical method using eggshells [106]. Results indicate that the grain size and crystallinity of the material is dependent upon the soaking time of CaO derived from eggshell in the K_2HPO_4 solution, where smaller sized particles were formed over longer soaking time resulting in slight peak broadening of XRD pattern. TEM and SEM analysis confirmed the formation of nanocrystalline circular particles.

2.7 Physicochemical and biological properties of HA

The present section will review the physical and mechanical properties of synthetic HA powders yielded from the implementation of the various HA powder production techniques (as discussed in the previous section). This section will aim to highlight the main differences between the HA synthesized to-date against that of biological HA (section 2.2).

2.7.1 Crystal Structure of HA

It is generally accepted that slightly nonstoichiometric HA has the hexagonal space group $P6_3/m$ structure, with a = 9.422 and c = 6.880 nm, while in the case of stoichiometric HA the structure becomes monoclinic $P2_1/b$ [108]. This is characterized by ordering within OH ion columns to form a sequence OH^- OH $^-$OH $^-$OH$^-$, with an ordered arrangement of these columns, so that the *b*-axis is doubled giving lattice parameters a = 9.421(8), $b = 2a$, c = 6.8814(7) nm, $\gamma = 120^3$ [107]. However, stoichiometric HA may also be hexagonal, if OH are disordered. Normally, only those preparations that have a final high-temperature stage have the possibility of yielding monoclinic HA. Other preparations are normally hexagonal, presumably because sufficient OH ions are missing, replaced by H_2O or impurity ions, so that the ordering is disturbed. Work carried out by the National Institute of Standards Technology (NIST) propose that the hexagonal form of HA is formed by precipitation from supersaturated solutions at 25ºC to 100ºC, while the monoclinic form of HA is primarily formed by heating the hexagonal form at 850ºC in air and then cooling to room temperature [109].

Recent theoretical studies find the hexagonal and monoclinic structures both energetically acceptable for HA [110], however some researchers finds that the $P6_3/m$ or the $P6_3$ hexagonal structural models are energetically unfavorable [111]. Rietveld analysis of X-ray diffraction patterns from a NIST standard reference specimen that HA (SRM-2910) crystallizes in a mixture of 23% $P2_1/b$ and 77% $P2_1$ monoclinic phases [131].

The overall XRD patterns of hexagonal and monoclinic HA are almost identical; however the pattern of monoclinic HA has additional weak lines whose intensities are less than 1% of the strongest hexagonal HA line [109].

There are two kinds of calcium-ion position contained in the lattice cell; hexagonal and columnar calcium. Hexagonal calcium ions (or six-calcium ions) are associated with these hydroxyls, forming equilateral triangles centered on and perpendicular to the hydroxyl columns. Six of the PO_4^{2-}tetrahedra are also on these planes. Columnar calcium ions being the net total of 4-calcium ions, are placed at the lattice points of [1/3, 2/3, 0] and [1/3, 2/3, 0] [113]. Table 2-2 outlines the lattice coordinates for its unit cell.

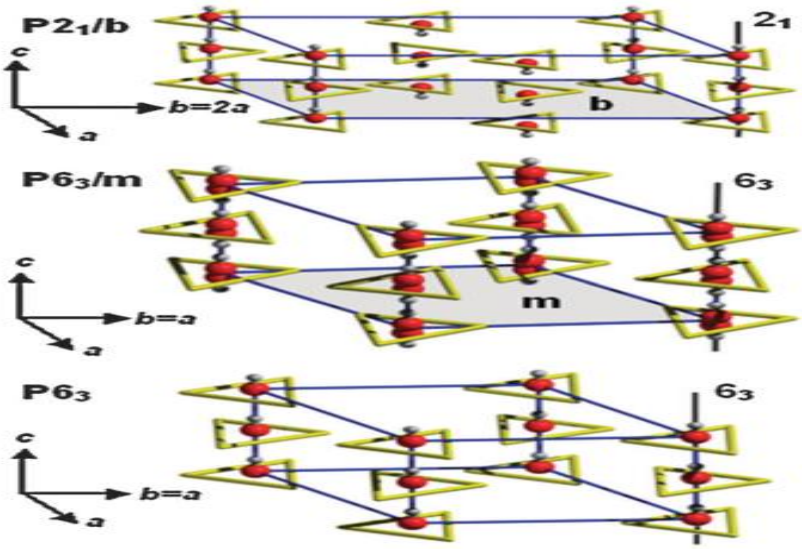

Figure 2-5: Various proposed HA structures: Monclinic (Top: $P2_1/b$), Experimental HA (Middle: $P6_3/m$) and Theoretical HA (Bottom: $P6_3$) Adapted from [112].

Table 2-2: Unit-cell positions of the HA lattice where; $\alpha=90^o$, $\beta=90^o$, $\gamma=120^o$ [35]

Atom	x/a	y/b	z/c
Ca(I)	1/3	2/3	0.0010
Ca(II)	0.2464	0.9938	¼
P	0.3999	0.3698	¼
O(I)	0.3272	0.4837	¼
O(II)	0.5899	0.4666	¼
O(III)	0.3457	0.2595	0.0736
Hydroxyl	0.0000	0.0000	0.1930

2.8 Process variables affecting the chemical precipitation method

2.8.1 Atmospheric Environment

During the chemical precipitation route, adsorption of atmospheric CO_2 may occur, which in the form of CO_3^{2-} anion can be incorporated into the HA crystal lattice, resulting in micro-stresses and distortion of the stoichiometric HA lattice [114]. However, within Nitrogen (N_2) controlled environments, small percentages of CO_3^{2-}

contamination was also found to arise as a consequence of subsequent sample handling steps [122].

Filtered inert gas should be continuously injected to both the reactor and the acid solution container during the precipitation process [121]. The filter should contain a sufficient amount of carbon dioxide absorber (such as, KOH or N_2). The HA powder can be very hospitable in the substitution of carbon dioxide in its crystal structure. CO_3^{2-} ions can substitute hydroxyls or phosphates sites and based on this substitution, type A and type B of carbonated HA are, respectively, formed. So, in order to reach a pure HA precipitate without any carbon dioxide contamination, it is effective to use controlled atmosphere during precipitation process. Filtered inert gas shall be continuously injected to the reactor and the acid solution container during the precipitation process. The filter should contain a sufficient amount of carbon dioxide absorber.

2.9 HA powder characteristics

The physicochemical properties for HA powders prepared from the chemical precipitation technique vary considerably due to the process variable conditions and raw materials used.

2.9.1 Crystallinity

Crystallinity depends on crystallite size and crystal strain and is the amount of crystalline phase present compared to its amorphous phase content. HA crystallization obeys the Ostwald rule of stages, so it is usually formed upon recrystallization of precursor phases such as OCP, DCPD and ACP [118]. There are two different crystallization processes involved in the crystallization of HA particles during synthesis and calcination. The crystallization of HA during synthesis follows a mechanism of solution crystallization. Since the crystal growth proceeds through the packing of HA molecules from the solution on the formed nuclei during the ripening process, the crystallites can freely grow on the surfaces of the precipitates in all directions. It is expected that the larger crystallites will be formed with longer ripening time until the crystallization reaches to its equilibrium. During calcination, crystallization of HA experiences both the nucleation and crystal growth by the rearrangement of HA molecules in amorphous phase. The nucleation and growth take place throughout the precipitates rather than on the surfaces only [118, 123, and 124].

As more HA molecules are available inside the precipitates for the nucleation and the crystal growth is in a confined environment, as well as the diffusion of the molecules in solid state is very slow, relatively smaller but more crystallites are expected to be produced in present calcination conditions. The dramatic increase in crystallinity after calcination indicates that the number of crystallites formed during calcination is large than that formed during synthesis, particularly for the "as prepared" HA powders with lower crystallinity. As a result, the apparent crystallinity post sintering (Xc) is reduced after calcination for the "as prepared" samples with high crystallinity and larger crystallites because a large amount of relatively smaller new crystallites are formed during calcination. On the other hand, the increased Xc for the "as prepared" samples with lower crystallinity and smaller crystallites comes from the growth of these smaller crystallites and new crystallites formed during calcination, which are relatively larger than "as prepared" smaller crystallites [124].

2.9.2 Particle Size

The synthesis of small HA powder particles (comprised of either smaller primary crystallites mentioned earlier or a mixture of primary crystallites with powder particles) are found to be attributed to the high super saturations derived from the high pH and short reactant addition time. An increased carbonate concentration may also contribute to the formation of small particles [94].

HA precipitated at 60°C had a particle size of 61.06 nm and at 80°C, a particle size of 82.24 nm, measured by line broadening effects [127]. Whilst the mean particle size for the HA precipitated at 80°C is larger, there appears in the TEM to be some fine particulate, which would stay in suspension more easily.

2.9.3 Particle Morphology

Spherical powders, in general, have better rheological properties than irregular powders and, thus, produce better coatings for hip implants and chromatographic separation [120]. The powders morphology will depend on whether the powder particle or crystallite size is being assessed. The temperature synthesis effect on the HA morphology indicates that at low synthesis temperature the crystals carry a needle shape [125].

Increasing the reaction temperature changes the crystal from as-needle shape to a more regular shape, close to circular. A shape factor can be defined by the ratio length/width of the Hap

crystals: Fs =L/1 (Fs: shape factor; L: particle length [m] and l: particle width [m]. The shape factor, Fs, of the HA crystals decreases with an increase of the synthesis temperature. After heating at high temperature T= 850ºC/ 4 h and then at T=1250ºC/ 4 h, the particle shape are with a more regular shape. After heat treatment at 1250ºC all the particles become thicker with a shape factor close to 1, this is due to the sintering of all the particles. Transmission electronic diffraction provides information at a one particle scale. The main axis of the HA particle with the needle shape corresponds to the c-axis of the HA structure. This is true for nanocrystals synthesized at low temperature (T 45ºC). Moreover the crystal looks like a monocrystal.

At higher synthesis temperature, nanocrystals are shown to lose their tendency to grow as a monocrystal following the c-axis of the apatitic structure. The crystallite size reaches a maximum value which corresponds to a temperature around 60ºC. This phenomenon can be explained by two temperature dependent effects which are concurrent. First of all, a temperature rise increases HA crystallinity which is thermally activated. Secondly, the temperature increase limits the tendency to the monocrystalline HA nanocrystals growth following the HA c axis, because from this critical temperature, particles become more regular and circular. Above this temperature, the tendency to grow stops. This explains the maximum size for the HA crystallites at this temperature. HA precipitated in work carried out at different temperature confirms that the reaction temperature significantly affects the precipitate morphology [127].

2.10 Infections in prosthetics and implants

Despite all the advances in the development of biomaterials, a significant number of implant procedures are affected by bacterial infection after implantation and revision surgeries as well as prolonged administration of antibiotics are required. Orthopaedic device-related infections (ODRI) are responsible for the failure of 1-2% of orthopaedic implants worldwide [129]. Implant joint infection is a relatively uncommon complication following hip and knee joint replacement and occurs approximately less than1 and 0.5%, respectively [130]. These infections may require prolonged therapy and often removal of the affected prosthesis is necessary [131, 132]. Infection may also occur early or late, from direct intra-operative inoculation, wound infection or haematogenous seeding. The most common infections are due to coagulase-negative staphylococci (CoNS) which are part of the normal flora of human skin

such as S. epidermidis, the most common CoNS pathogen that accounts for about 74% to 92% of all hospital-acquired CoNS infections and S. haemolyticus, the second most common CoNS, often a pathogen in endocarditis, septicemia, peritonitis, urinary tract infections, osteomyelitis, and wound infections. Other common pathogens include S. aureus,enterococci, streptococci, corynebacteria, enterobacteriaceae and anaerobes [133]. Infection occurs when bacteria are attached to the implant surface and biofilm, which is a resistant form of bacterial colony, starts to form. The biofilm develops through the following stages:

I. Surface adhesion followed by
II. Multilayered cellular proliferation and
III. Intercellular adhesion in an extracellular polysaccharide matrix.

Generally the body immune system cannot prohibit bacterial proliferation when a protective bacterial biofilm layer has been already formed [134]. Hence, it is critical to prevent the initial colonization and adhesion of bacteria in order to control infection.

Pathogenic microorganisms, particularly gram-positive S. aureus and S. epidermidis, have been found in approximately 90% of implants [128]. Gram-negative E.coli, Pseudomonas aeruginosa, and the pathogens from the Proteus group (e.g., P. mirabilis and P. vulgaris) have also been found in implant-associated infections [128]. Implant infections are not only due to a poor surgical operation or host health factors (such as obesity or chronic diseases) but can also arise from the anatomical characteristics of the implant site and properties of the implanted device such as its size and shape [135].

Another major concern in recent years has been the increasing occurrence of infections from antibiotic-resistant bacteria. In a large surveillance in surgical site infections after orthopaedic interventions, 59% of the infections were due to the isolated methicillin-resistant S. aureus (MRSA) strains. The reported incidences of MRSA infection at the surgical site increased from 32% to 64% between 1992 and 2003 [138]. MRSA is associated with higher rates of patient morbidity and mortality than non-MRSA strains [139] and its control demands for new antibiotics or using alternative agents with minimum or no bacteria resistance (such as zinc nanoparticles).

Hence, the local delivery of drugs to bones or infected implant site is becoming more popular for the treatment of post-operative complications. This to a large extent can be achieved by preloading implants with antimicrobial agents, which can reduce the systemic body burden of drugs. For example, bone cements are often preloaded with antibiotics as a standard practice [140].

2.11 Mechanism of antibacterial/antimicrobial activity of metal ions

Figure 2.5 illustrates a possible mechanism of antibacterial activity of ions, where the exact method of interactions is not fully determined. There are three mechanisms, which are thought to explain how ions can prohibit the growth of microorganisms:

I. Penetration of ions through the cell membrane and change the regulation of ATP production and DNA replication,

II. Ion attachment to the cell membranes with electrostatic forces, which disrupts the integrity

of the cell and also affects the free transportation of protons and other molecules in and out of cell, and

III. Induction of an oxygen stress by formation of free radicals (also called reactive oxygen species: ROS) which interfere in the normal function and can irreversibly damage bacteria (e.g. their membranes, DNA and mitochondria), resulting in bacterial death.[142].

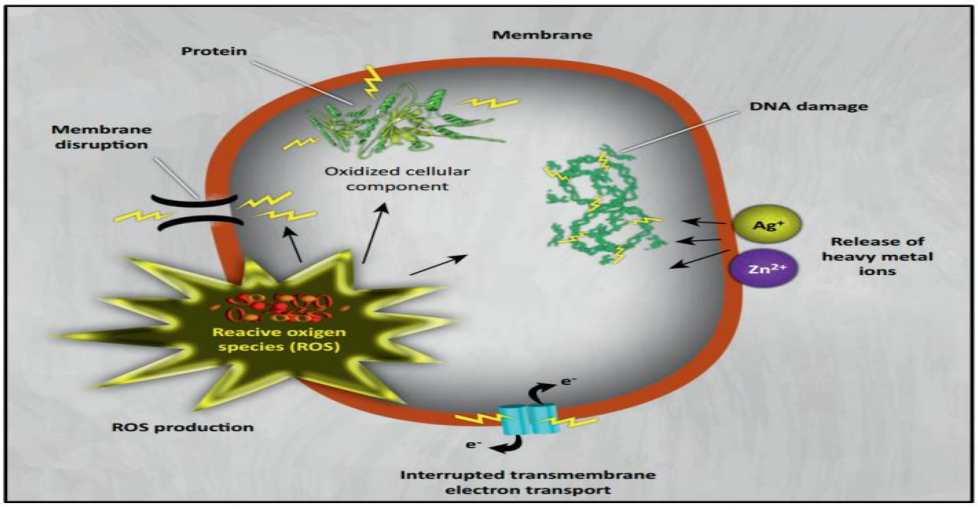

Figure 2-5: Antibacterial mechanisms of nanoparticles and their ions, adopted from [142].

Further studies have also reviewed other possible interactions of metal ions with bacterial cells to explain their antibacterial activity. Kandile et al. [143] proposed that heavy metals can react with proteins via thiol (SH) groups leading to inactivation of proteins, but as explained earlier, the general concept is that silver nanoparticles follow mainly the mechanisms discussed above.

Zn substituted HA (Zn-HA)

The mechanism of the antibacterial activity of HA with zinc ions is again not yet fully understood. It is proposed that Zn ions form strong bonds with thiolic, imidazole, amine, and carboxylic groups of proteins, causing structural changes and also affects the membrane permeability and transport resulting in cell death [167, 168]. It is also shown that Zn ions can damage the enzymatic activity and DNA and RNA of bacteria with similar results [147].

In addition to its role as an antimicrobial agent, Zn-HA ceramics are used to regulate other biological functions. Composite ceramics of Zn-TCP/HA as implants in the femor of New Zealand White rabbits for 4 weeks and reported increasing rates of bone formation at concentrations of 0.316 wt. % [148].

Some reported, that the addition of Zn-HA decreased the inflammatory reaction following the implantation of HA based prosthesis by increasing the production of cytokines [149]. Generally Zn substituted HA could consist of a new generation of biomaterials for bone tissue engineering [144].

Finally, according to survey of literatures, some works need to be done related on extracting calcium source from waste materials and at the same time achieving properties like antibacterial behavior. Therefore in this study it is planned to fill that gap.

CHAPTER THREE

MATERIALS AND METHOD

Materials required for synthesis are:-

1. Chicken Egg (Elfora Agro Industry)
2. Nitric Acid (HNO_3) (LOBA CHEM, 70%)
3. Diammonium Hydrogen Phosphate ($(NH_4)_2HPO_4$) (UNI-CHEM, 98.5 %)
4. Zinc Nitrate tetra hydrate ($Zn(NO_3)_2.4H_2O$) (LOBA CHEM, 99%)
5. Ammonia Solution (NH_4OH) (35%)

The experimental procedure is listed below:-

1. Chicken egg shells were first cleaned in boiling water two times and put in oven. The average mass of the single egg shell was 8.5 gram.

Figure 3-1: After the egg is broken and organic part removed from inside

Figure 3-2: Egg shells being cleaned using boiling water

Figure 3-3: crushing the cleaned egg shell for calcination

2. Then dried clean shells were analyzed using XRD and proven to be calcium carbonate.
3. To calcine the shells Thermogravimetric Analysis (TGA) were made, and calcination temperature chosen to be 900 ^{o}C by crosschecking literatures [87, 96]. Hence the shells are calcined at 900 °C (heating rate of 10 °C/min) for 1 hr using electric furnace in air. The calcined powder is ground in an alumina mortar–pestle.

$$\boldsymbol{CaCO_3 \xrightarrow{900\,^{o}C} CaO + CO_2} \qquad \boldsymbol{3-1}$$

(Egg shell)

4. The Calcined powders were then analyzed using XRD and proven to be calcium oxide (CaO)
5. Then to make calcium nitrate using the calcined eggshell (calcium oxide), Eq 3-2 below was used as base. Therefore by considering the 1:2 mol ratio of calcium oxide with nitric acid, for 3 grams of calcium oxide and 9.5ml of nitric acid was used. First the concentrated nitric acid was taken and heated at 40 ^{o}C in hot plate and stirred for 3 min, then calcium oxide was put to the acid using spatula and dissolved until the pH neutralized. After complete dissolving, the solution is stirred and heated at 60 ^{o}C, and finally calcium nitrate precipitates were found. For the above mentioned amount of reactants, 0.0536 mol of calcium nitrate product is formed. This calcium nitrate is used for the synthesis of hydroxyapatite later.

$$\boldsymbol{CaO + 2HNO_3 \rightarrow Ca(\,NO_3\,)_2 + H_2O} \qquad \boldsymbol{3-2}$$

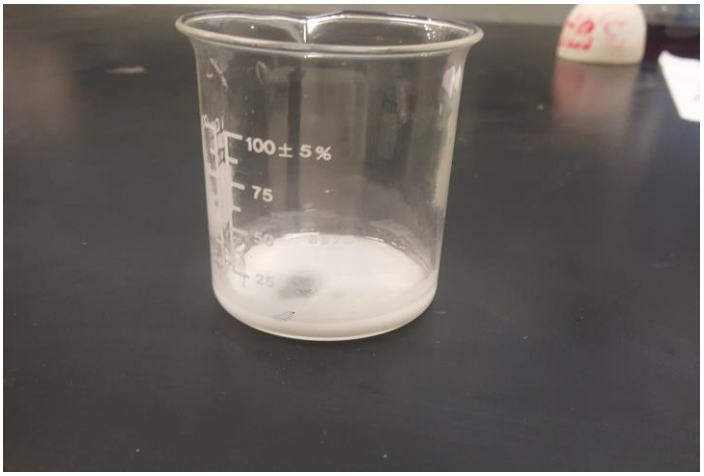

Figure 3-4: Precipiates of calcium nitrate

6. The principle of synthesizing divalent cation (M^{2+}) substituted HA by wet chemical method is expressed in the following equation [73] :

$$(10-x)Ca^{2+} + xZn^{2+} + 6PO_4^{3-} + 2OH \rightarrow Ca_{10-x}Zn_x(PO_4)_6(OH)_2\ (0 \leq x \leq 10) \qquad 3-3$$

The general equation of reaction is as follows [73]

$$Ca(NO_3)_2.4H_2O + Zn(NO_3)_2.6H_2O + (NH_4)_2HPO_4 + NH_4OH \rightarrow Ca_{10-x}Zn_x(PO_4)_6(OH)_2 \ (Hydroxyapatite) \quad 3-4$$

Table 3-1: Code Naming of samples

Code Name	Meaning
HA	Pure HA, without Zinc Substitution
Z0.3HA	HA, 0.3 mol% substituted
Z0.6HA	HA, 0.6 mol% substituted
Z0.9HA	HA, 0.9 mol% substituted
Z1.2HA	HA, 1.2 mol% substituted

N.B:- From this onwards the above nomenclature will be used to identify the samples.

- The precursors for the synthesis of hydroxyapatite amount are calculated according the Eq 3-3, in which the calcium nitrate to diammonium phosphate molar ratio is 10:6 to form hydroxyapatite [73]. Therefore in this synthesis to satisfy the 10:6 ratio of calcium to phosphate, 100 ml aqueous solution of diammonium phosphate is prepared with 0.12 M concentration and 100 ml aqueous solution of calcium nitrate was prepared with 0.2 M concentration. In which calcium to phosphate ion mole ratio is 1.66.

- The substitution of zinc to hydroxyapatite was based on the idea, zinc will replace the calcium place in the hydroxyapatite [154, 156]. Therefore the diammonium phosphate amount was fixed, and the calcium nitrate amount was changed for various ratio of zinc addition. Zinc substituted HA's with various x values (0, 0.03, 0.06, 0.09 and 0.12) in Eq 3-3, in other word this mean (0, 0.3, 0.6, 0.9, 1.2 mol %) substituted zinc to the HA.

- Ammonia solution 28% was used as a PH regulator in the later synthesis, Therefore 35 % stoke solution of ammonia that is purchased was diluted to 28%.
- The synthesis was started by adding Diammonium phosphate $(NH_4)_2HPO_4$ solution into Calcium nitrate/zinc nitrate solution, by drop wise fashion (using burret), while keeping the solution PH at 10 by adding small amount of the ammonia solution.

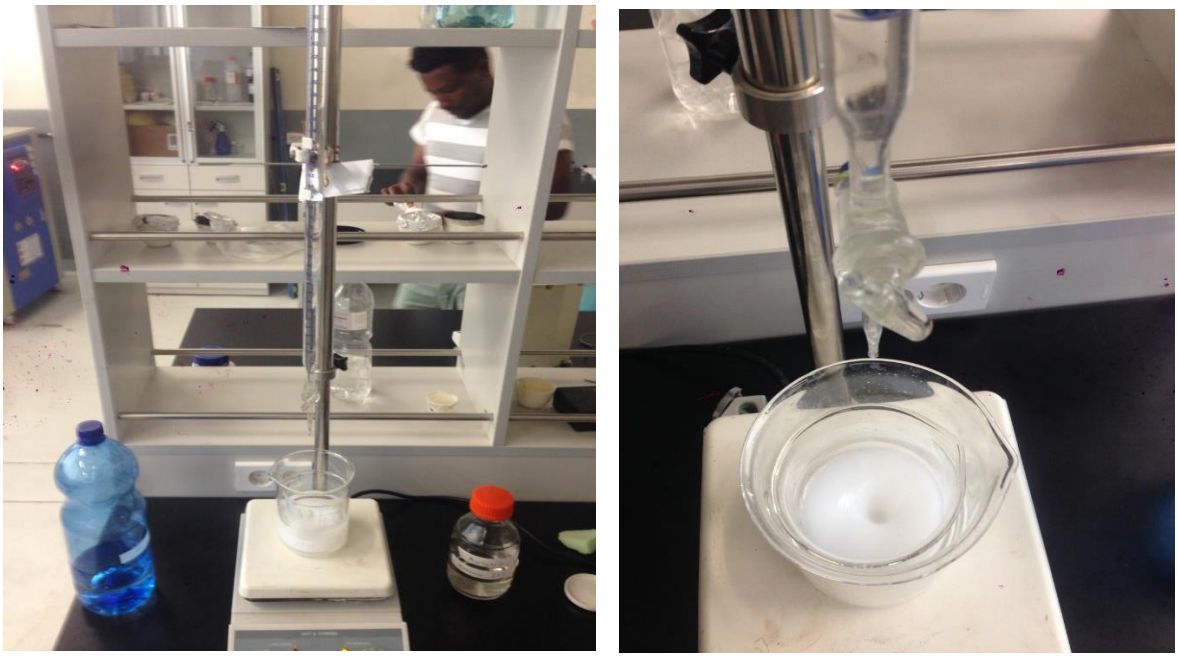

Figure 3-5: Drop wise addition of Diammonium phosphate in the burret to calcium nitrate/zinc nitrate solution in the beaker under vigorous stirring

- After adding the Diammonium phosphate, the solution was heated at 90 ^{o}C for 5 hours under constant stirring of 100rpm. The precipitates were then filtered and washed three times by distilled water with ultra-sonication.

Figure 3-6: filtering using filter paper the final precipitates

- Finally the precipitates were dried in an oven at 100 ^{o}C for 12 hours.

Characterization was made by the following instruments and procedures.

X-Ray Diffraction

X-ray diffraction (XRD) is a versatile, non-destructive instrument that is used for determination of atomic arrangement within a material, giving the crystalline phases from the atomic spacing and symmetry [150]. In this technique, X-rays of a known wavelength are passed through a sample to fully investigate its crystalline structure. The wave nature of the X-rays means that they are diffracted by the lattice of the crystal to give a unique pattern of peaks of 'reflections' at differing angles and of different intensity, just as light can be diffracted by a grating of suitably spaced lines. The diffracted beams from atoms in successive planes cancel unless they are in phase, and the condition for this is given by the Bragg's relationship:-

$$n\lambda = 2dSin\theta \qquad 3-5$$

Where; λ is the wavelength of the x-rays, d is the distance between different plane of atoms in the crystal lattice and θ is the angle of diffraction.

Prior to XRD analysis, the samples were ground using a marble mortar and pestle before distributing 200mg of the ground sample powder over a 10mm diameter circular area of 25mm.The prepared HA samples were analyzed by XRD device (XRD-7000S, Dangil SHIMADZU) using a high resolution with CuKα monochromatic beam (wavelength=0.154056 nm) produced at 40 kV and 30 mA.

Phase Identification

For the phase identification step, the X-ray diffraction patterns were directly compared to the files for HA from the Joint Committee for Powder Diffraction Standards (JCPDS, Card No. 09-432) as was supplied by the International Centre for Diffraction Data (ICDD).

Crystal size

The crystal size, of the precipitates was estimated from XRD pattern using the Scherrer's formula [151]. According to this equation, a single crystal dimension perpendicular to the (h k l) plane (D_{hkl}) (nm) can be estimated from the peak broadening as:

$$D = \frac{K\alpha}{\beta * Cos\theta} \qquad (Scherrer's\ formula) \qquad 3-6$$

Where D is the crystal size in nm; K is the Scherrer constant (0.9 for hexagonal HA), α- is the wavelength of the monochromatic X-ray beam (0.15418 nm); β is the FWHM is the experimental Full Width at Half Maximum intensity of the diffraction peak under the consideration peak; θ is the diffraction angle (°). In samples with apatite structures, the line broadening of the (002) reflection was used to evaluate the mean crystal size, which corresponds to the *C* crystallographic axis.

The lattice parameters determination

The spacing of the lattice points in a crystal is an important quantitative aspect of its structure and its investigation by X-ray diffraction. In case of the hexagonal crystal structure of HA, the lattice parameters were denoted by (a=b), and c and were determined from the relationship between the distance (d) of two adjacent planes and the (h k l) Miller Indices by using the equation below [171]:

$$d = \frac{1}{\sqrt{\frac{4(h^2 + hk + l^2)}{3a^2} + \frac{l^2}{c^2}}} \qquad 3-7$$

Where d is the lattice spacing, h, k, l is the Miller indices, *a*, *c* is the lattice parameters, λ is the wavelength (CuKα: λ = 0.154nm) and 2θ is the diffraction angle. For the hexagonal unit cell, a = b, α = β = 90º, and γ = 120º

FTIR-Fourier Transform Infrared Spectroscopy

Fourier transform infrared spectroscopy (FT-IR) is a chemical analysis technique that generates a molecular fingerprint of the samples. It is based on the vibrations of the atoms, which are subjected to a passing infrared radiation and measures the ratio of the incident radiation is absorbed at a particular energy [152]. As the sample is exposed to different wavelengths of infrared light, transitions between vibrational energy levels of various chemical bonds are detected, allowing for the functional groups within the molecules of the sample to be identified. The resulting spectra, which are a characteristic of infrared absorption/emission at different wavelength, can be used to define the chemical composition of the sample.

In this study, FT-IR was used for further confirmation of the chemical composition of the samples. FT-IR spectroscopy was handled by Spectrum 65 FTIR (PerkinElmer)

Sample preparation consisted of mixing 2mg of each sample with 300mg of Potassium bromide (KBr), compressed to form a tablet and then placed on specimen holder for analyzation from 400 to 4000cm^{-1}.

Thermogravimetry Analysis (TGA)

TGA is used to study the change in mass of a sample as the temperature is varied. By controlling the atmosphere e.g. with O_2 or N_2, it may be possible to encourage or suppress oxidation reactions, thus controlling to some extent the nature of the thermal events occurring [153]. When heated to 1000°C, many materials undergo weight changes giving characteristic curves. Where the changes can be linked to the particular thermal events, such as oxidation, or loss of water of crystallization, the size of the step in the curve can be used for the quantitative analysis.

TGA analysis was carried out in a SHIMADZU DTG-60PLUS instrument, under air atmosphere with the heating rate of 10°C/minute. 100mg of dried samples were grinded to make a fine powder.

Antibacterial Analysis

Method used > Disc Diffusion (Kirby Baure disc diffusion)

Diluent used >DMSO (Dimethyl sulfoxide)

Standard for dilution used > 0.5 McFarland Standard, which corresponds to 10^5-10^7 bacteria/ml or in average 10^6 CFU/ml (colony forming unit per milliliter.

Figure 3-7: McFarland Standard, standard used to dilute a bacteria

Dilution type > serial dilution

Volume Used > 5µl of the dissolved HA

Figure 3-8: Sample prepared with a serial dilution from HA powder samples

Bacteria used > two types of organisms

One gram positive > Staphylococcus aureus (S aureus)

One gram negative > Klebsiella pneumoniae (K Pneumoniae)

Media Used > Mueller Hinton Agar

Procedure

1. The Mueller Hinton Agar was prepared
2. The bacteria were taken by cotton tip swamp and inoculated into the media

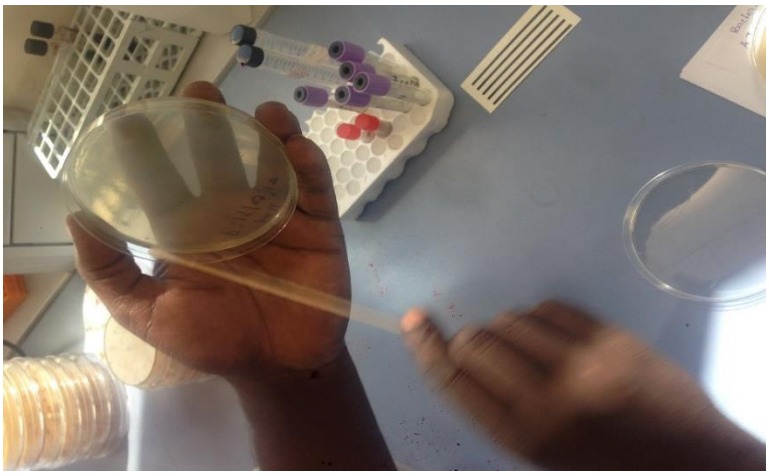

Figure 3-9: Inoculation of the bacteria into the dish

3. Watman filter paper put in the dish after sterilization by hook (as identifier)
4. Then drop on the diluted 5µl compound was made in the watman paper
5. Finally the dish was incubate at 37^{o}C for 18-24 hours with oxygen feed
6. On the next day inhibition zone was read.

CHAPTER FOUR

RESULT AND DISCUSSION

4.1 XRD characterization

The XRD analysis of the egg shell:-

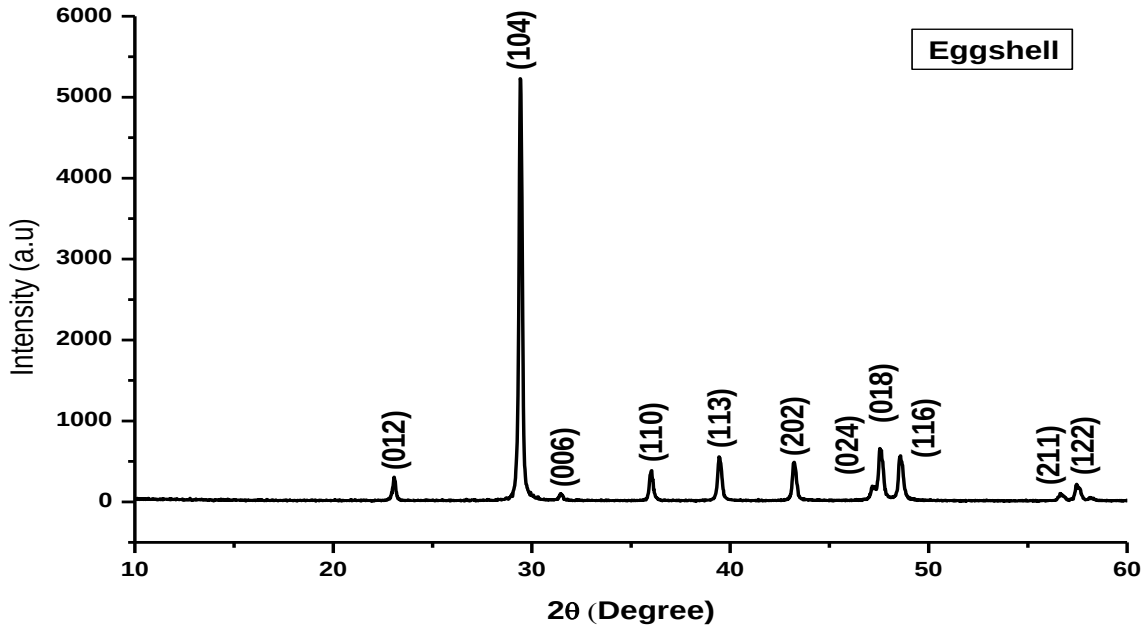

Figure 4-1: The XRD diffraction patterns for eggshell

The calcined eggshell result is:

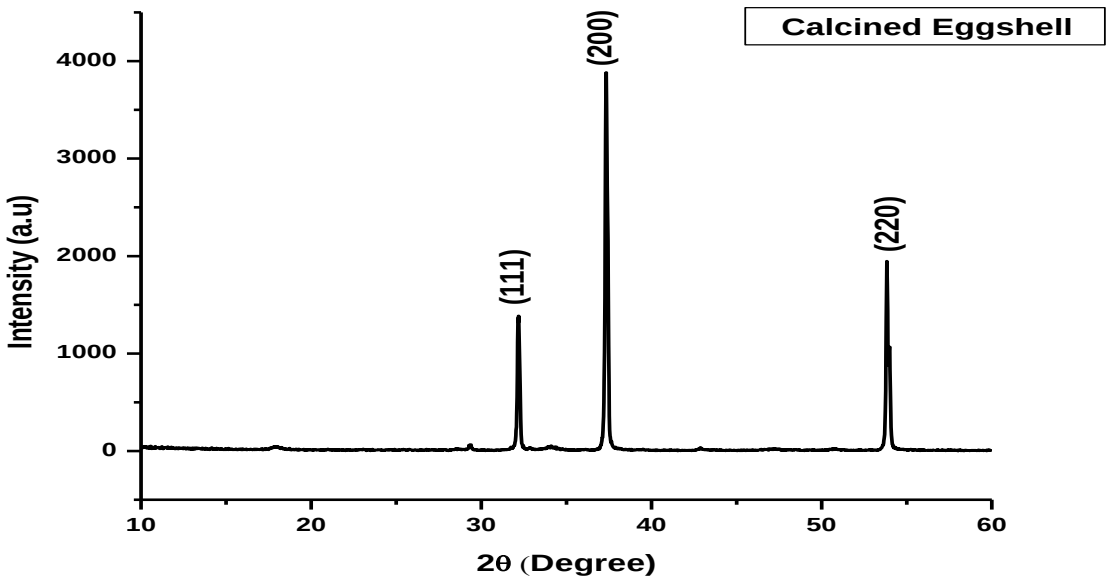

Figure 4-2: The XRD diffraction patterns for calcined eggshell

4.1.1 Calcium precursor analysis

The XRD diffraction of the cleaned and crushed eggshells is shown on figure 4-1. It shows that peaks of $CaCO_3$ are observed in the structure of the egg shell with a hexagonal structure, where the highest intensity peak is observed at a 2θ angle of 29.43 corresponding to a Miller indices of (104), referring to the ICDD card of 5-0586.

The Calcination temperature for $CaCO_3$ to CaO conversion, has been reported commonly at 900^{o}C [96, 106]. Therefore the calcination temperature was chosen at 900^{o}C, Figure 4-2 shows the XRD diffraction of the calcined egg shell that is calcium oxide, showing the highest intensity CaO peak with cubic structure is observed at a 2θ angle of 37.35^o corresponding to the (200) lattice plane, referring to the ICDD card of 037-1497.

- The XRD data for the Precipitates of the Hydroxyapatites and its zinc-substituted counterparts are:-

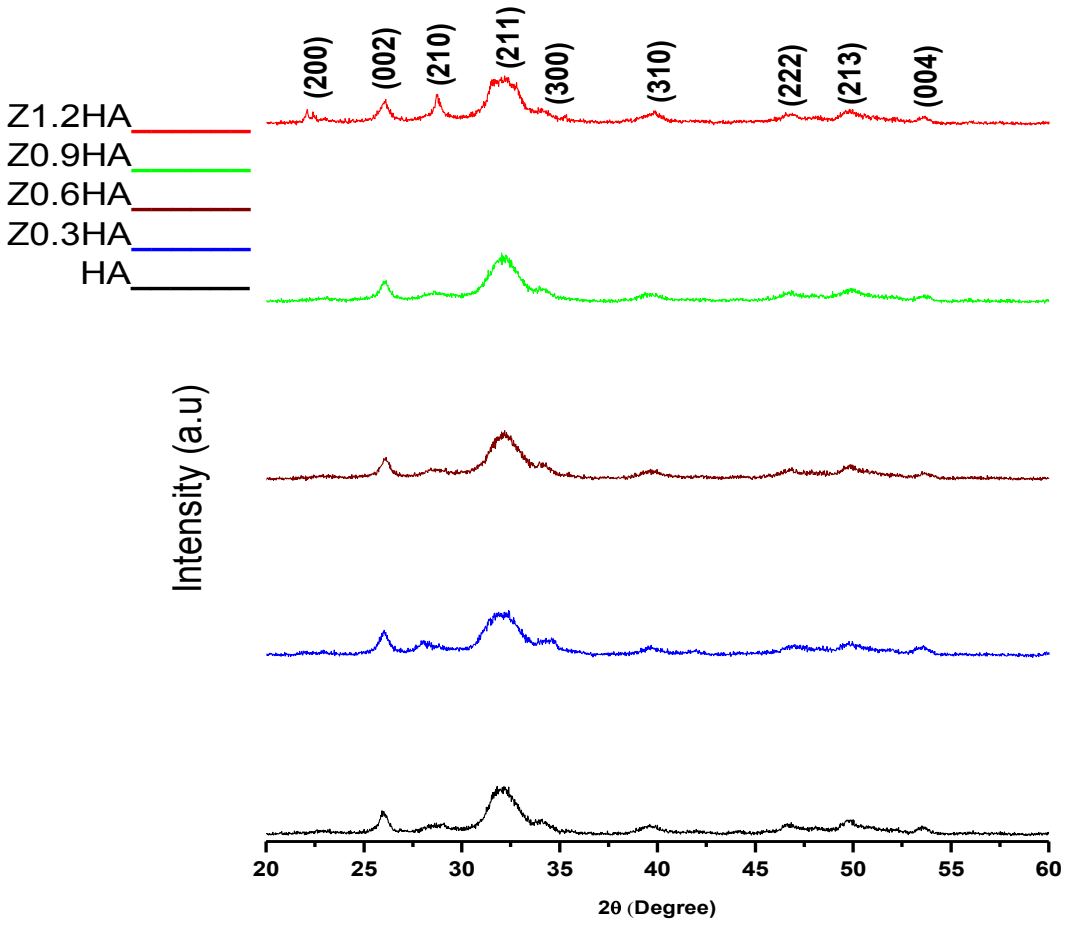

Figure 4-3: The XRD diffraction patterns for pure HA and zinc-substituted HA with different ratio

4.1.2 Phase analysis of HA precipitate extracted from eggshell

The XRD pattern of the synthesized HA precipitate powder, from the pure to different zinc substitution ratio, shown in Fig. 4-3. The highest intensity peak was observed at a 2θ angle of 31.14°, corresponding to miller indices of (211), referring to the ICDD card of 09-432.All peaks were indexed to hexagonal Hydroxyapatite without secondary phases such as α-TCP and β-TCP. This demonstrated the successful synthesis of pure phase HA via the chemical precipitation technique, for the unsubstituted hydroxyapatite and up to 1.2 mol % ratio, zinc-substituted hydroxyapatite, all extracted from the eggshell.

Crystal size: of the precipitates was estimated from XRD pattern using the Scherrer's formula ($Equation\ 3-4$)

Table 4-1: Crystal size of Zn-HA

Sample	Line width (0 0 2) FWHM (°)	Line width (0 0 2) FWHM (rad)	Average crystal size D(Å)
HA	0.566440	0.009886	143.89
Z0.3HA	0.649522	0.011336	125.48
Z0.6HA	0.676244	0.011802	120.52
Z0.9HA	0.728859	0.012721	111.82
Z1.2HA	0.747967	0.013054	108.97

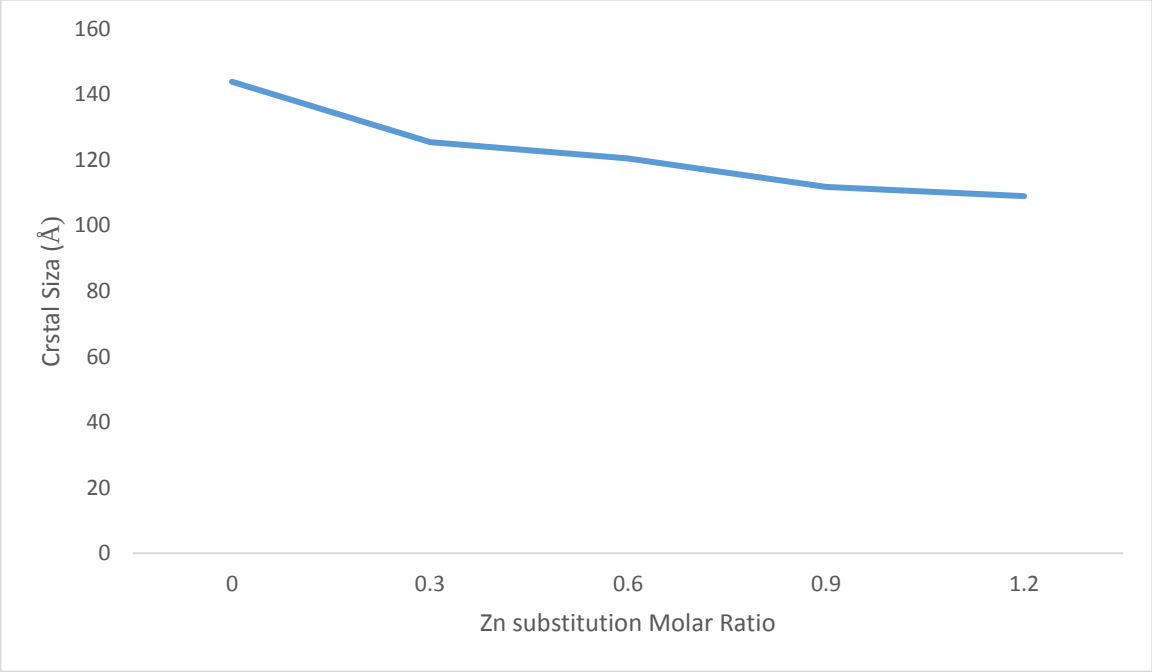

Figure 4-4: Crystal size of Zn–HA as a function of Zn content.

Table 4-2: Lattice parameter of Zn-HA. (Error, 0.003±)

Sample	a(Å)	b(Å)	c(Å)
HA	9.431	9.431	6.890
Z0.3HA	9.424	9.424	6.884

Z0.6HA	9.419	9.419	6.875
Z0.9HA	9.410	9.410	6.840
Z1.2HA	9.375	9.375	6.810

Crystal size:

The crystal size of the precipitates was calculated by scherrer's formula using the XRD data as shown in figure 4-4. It can be observed that the crystal size decreases as the zinc substitution ratio increases, from 14.3nm to 10.9nm. This is due to the inhibition of zinc to crystal growth of HA [67, 68 and 73], and also statistic disorder in the hexagonal channel due to the Zn insertion [154].

Lattice parameter, was calculated using the XRD data on Eq 3-5 and Eq 3-7. And it is observed that a and c lattice parameters decrease when the zinc substitution amount increased. This implies the incorporation of zinc into the hydroxyapatite. The reason for the decease of the lattice parameter is due to lower ionic radius of Zn^{2+} (0.0745 nm) when compared to Ca^{2+}ions (0.99 Å) [56].

4.2 FTIR Analysis (Fourier-transform infrared spectroscopy)

The samples tested are , pure HA extracted from egg shell, 0.3, 0.6, 0.9 and 1.2 mol % zinc substituted Hydroxyapatites extracted from egg shell.

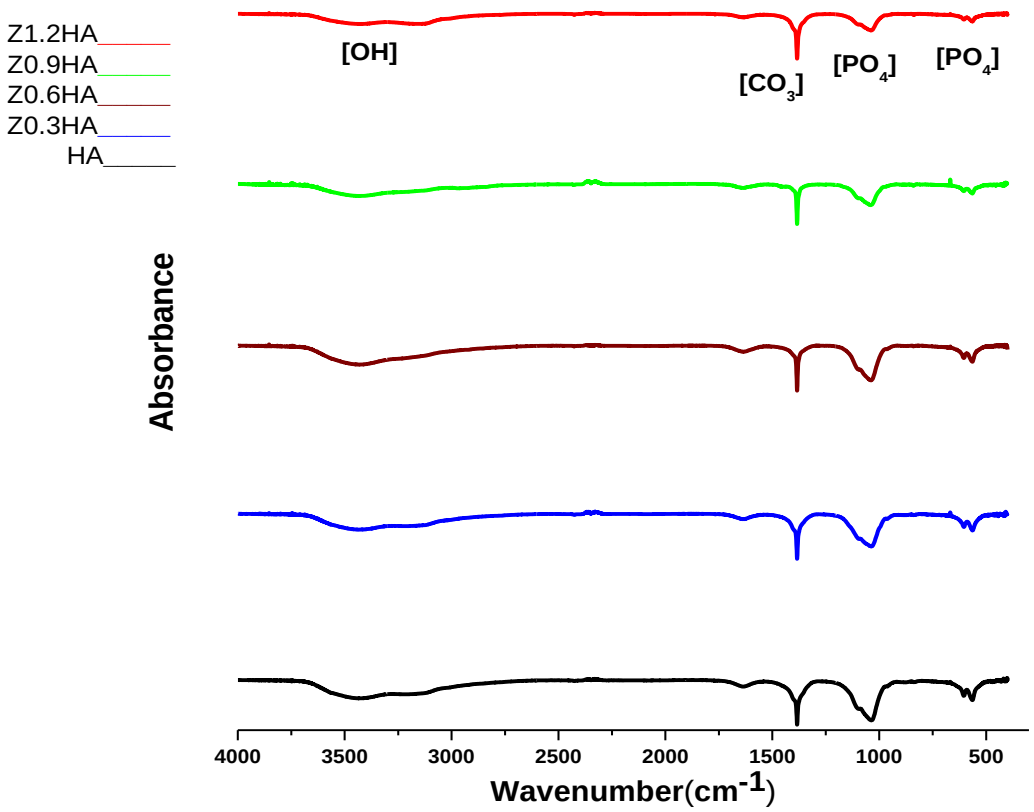

Figure 4-5: FT-IR spectra of zinc substituted hydroxyapatite with different Zn concentrations.

Figure 4-5: presents the frequency bands corresponding to vibrational groups inherent to the structure of HA and Zn-HA.

The proof for presence of apatite phase in the final powder can be established by the presence of fundamental vibrational modes of PO_4^{3-} group at bands 574, 609, 966 and 1020-1120 cm^{-1} [155]. The bands at 3570 cm^{-1} are representative of OH group in the apatite phase while the adsorbed water can be seen in the region around 3300-3600 cm^{-1}. The presence of carbonate CO_3^{2-} groups at 1430 cm^{-1} can be due to the adsorption of soluble carbon dioxide originating mainly from air during the aqueous precipitation as the experiments were not carried out in an inert environment. [155]

FT-IR analysis showed that partially carbonated hydroxyapatites has been formed, based on a strong carbonate-specific bands in the range of 1460–1410 cm-1 indicating that carbonate groups have substituted PO_4^{3-} in the hydroxyapatite lattice.

A small peak at 1635 cm^{-1} and a stretched band, between 3000 -3600 cm^{-1} is expected to be caused by "bound" water or hydration layer, which was present in all the FT-IR spectra and is associated with HA crystals. [155]

FT-IR for Zinc substituted *HA:* - The zinc doesn't show any significant change to the FT-IR spectra, which means we have additional information to XRD data that we have pure phase of apatite. But as we observe from the unsubstituted to substituted HA with different ratio, we notice that of the bands at 473(v2), 566 and 604(v4), 962(v1), 1020-1120 cm^{-1}(v3) were characteristic to phosphate groups. With the increase of Zn molar fraction, the peak intensity of OH, v1 PO_4 and v2 PO_4 group tends to be less. These changes suggest the crystallinity of the apatite decreased and are consistent with the results of crystal size calculation from the XRD analysis [156].

4.3 Thermal Analysis

The Thermogravimetric analysis (TGA) of the HA powder was carried out between the room temperature and 1100°C in order to understand the phase transformation within the samples in relation to temperature.

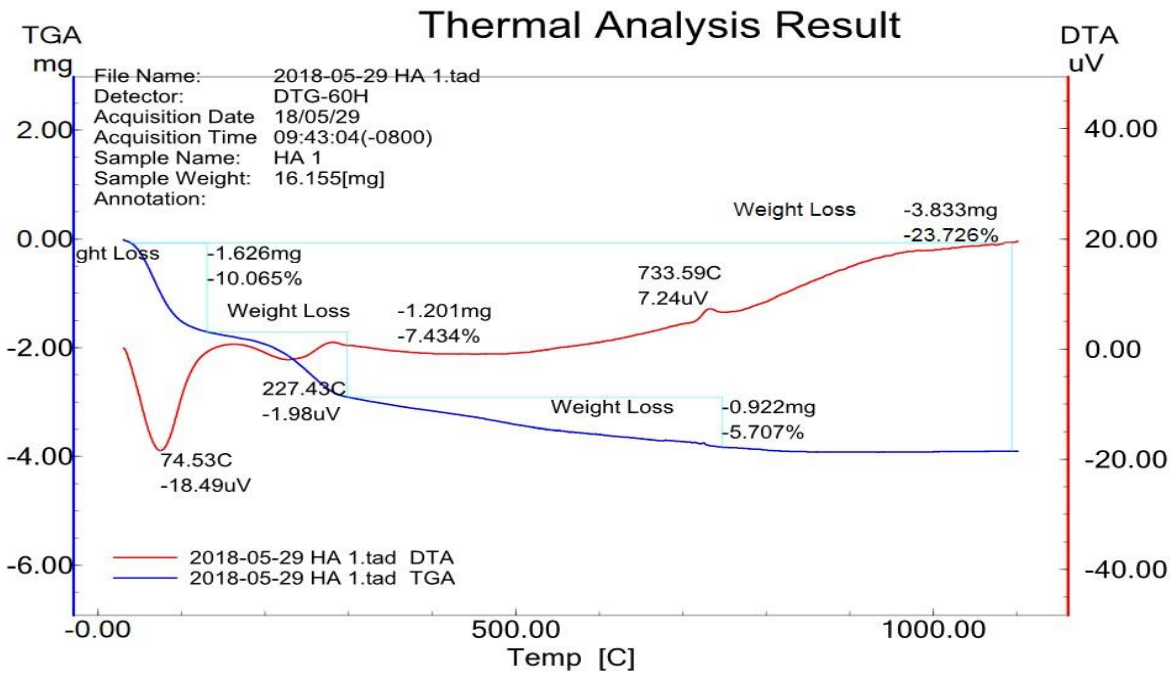

Figure 4-6: TGA graph of hydroxyapatite

The TGA results for HA sample are shown in Figure 4-6.

Table 4-3: Behavior and weight loss of HA sample in relation to temperature

Sample Temperature (^oC)	Behavior	Weight loss
25-100	Removal of absorbed water from surface	10.06 %
100-400	Removal of absorbed water in the lattice	7.434
400-700	Decarbonation	5.7 %
700-760	Dehydroxylation	0.52%
760-1100	Decomposition (Transformation from HA to TCP)	

The reaction is shown in the following equation:-

$$Ca_{10-x}Zn_x(PO_4)_6(OH)_2 \rightarrow 3Ca_3(PO_4)_2 + CaO + H_2O \uparrow \qquad 3-5$$

Hydroxyapatite $\rightarrow$TCP (TriCalcium Phosphate)

The decomposition of HA is promoted by the presence of more Zn substitution which means that Zn substitution destabilizes the apatite structure [157].

The total weight loss was about 23.7 % for HA sample.

Therefore, according to the TGA analysis, it is recommended that to heat treat the prepared precipitate powders around 450-500^oC.

4.4 Antibacterial Analysis

The inhibition zone was taken photograph and zone of inhibition calculated for both bacteria.

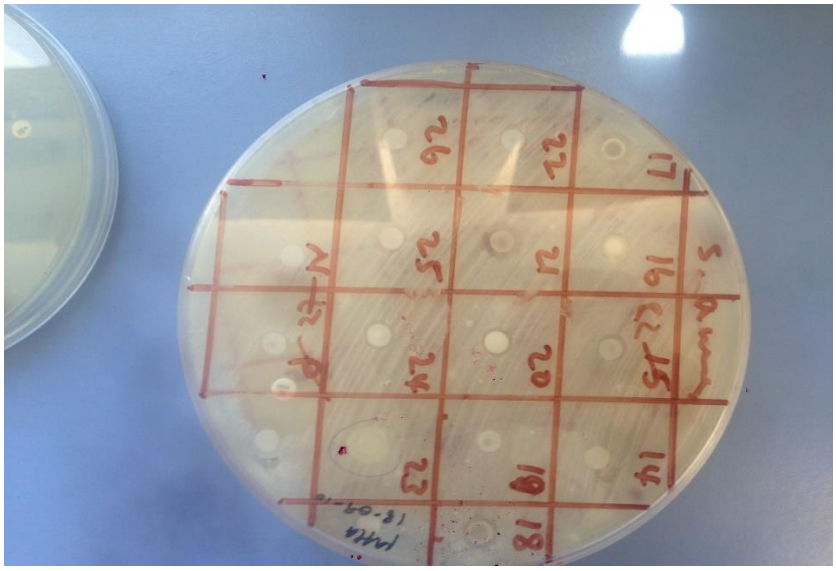

Figure 4-7: Zn-HA samples DD test for S aureus

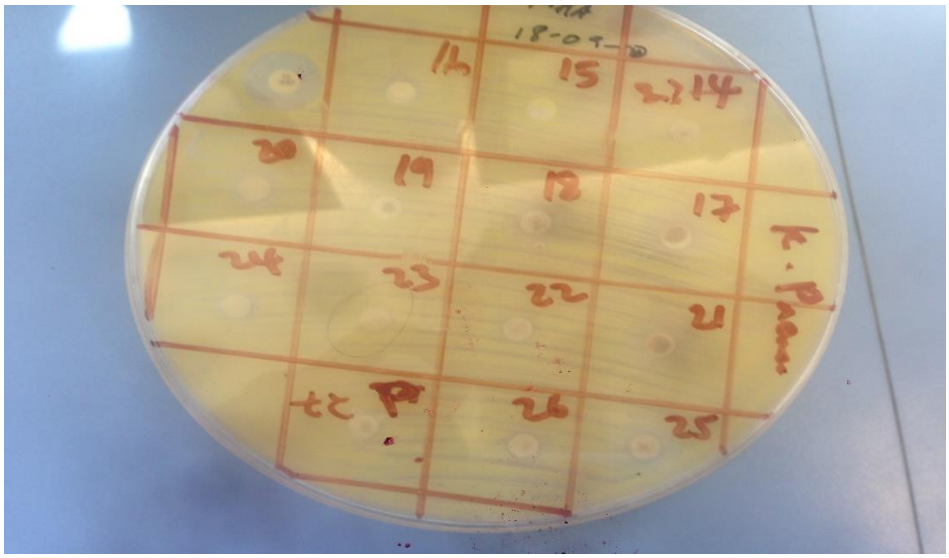

Figure 4-8: Zn-HA samples DD test for Klebsiella pneumoniae

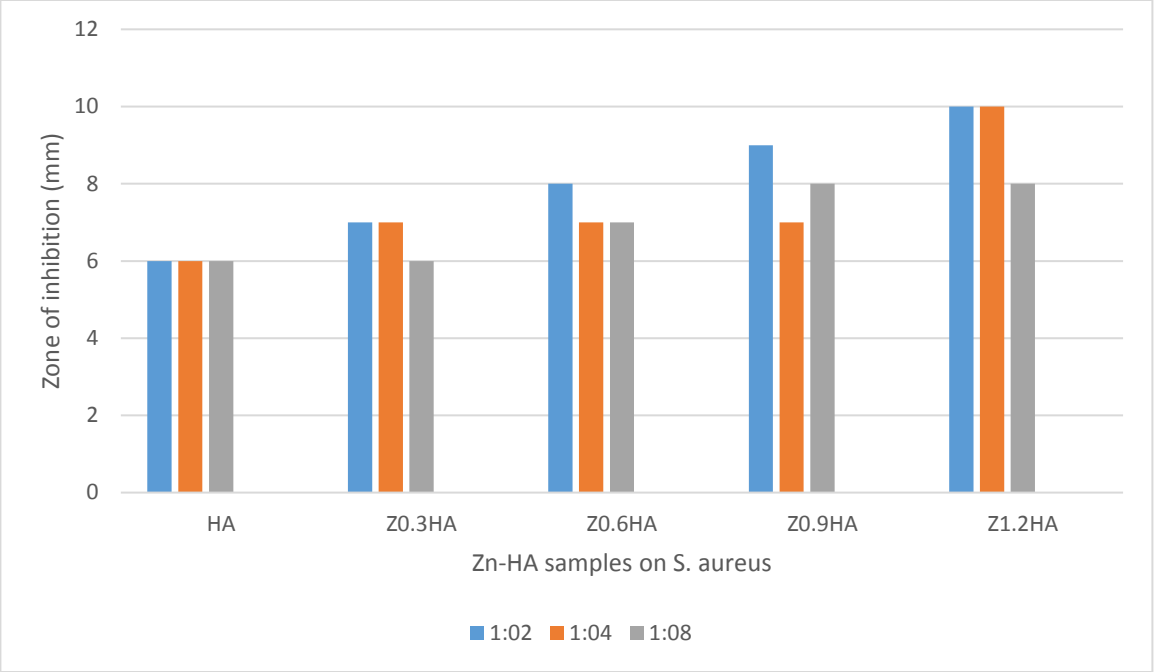

Figure 4-9: Zone of inhibition read data for Zn-HA samples on S.aureus bacteria

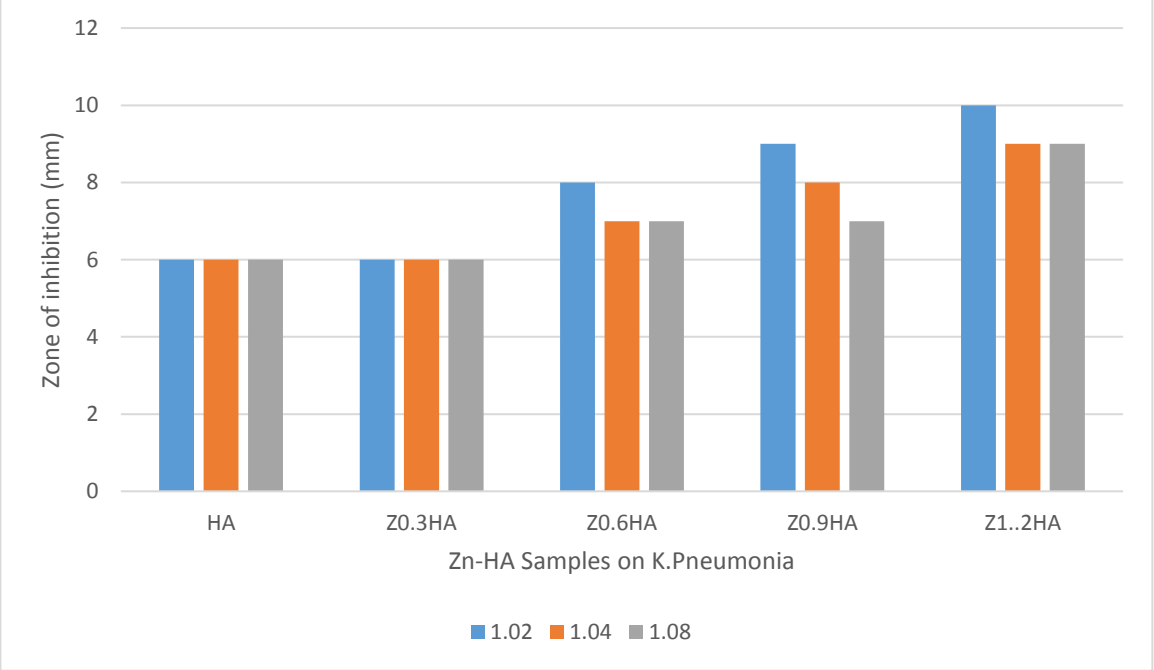

Figure 4-10: Zone of inhibition read data for Zn-HA samples on K.Pneumonia bacteria

Measuring antibacterial activity of Zn-HA samples

The advantages of using inorganic particles (e.g. Zn) as antimicrobial agents are their greater effectiveness on resistant strains of microbial pathogens, less toxicity and heat resistance [158]. It is also a crucial molecule for human cells, particularly bone cells, and can exhibit strong activity at very low concentrations [159, 160]. Zn is known to be in the active center of more than 300 enzymes involved in bone metabolism [161].

The antibacterial activity of HA and zinc substituted (as in 0, 0.3, 0.6, 0.9 and 1.2 mol %) were teste by disc diffusion method (DD).

The antibacterial property of Zn increased with a higher concentration in the solid sample. The presence of a ZI (Zone of inhibition) clearly indicates that Zn ions are released from the solid specimen into the agar and have an antibacterial effect against both strains.

Previous works have confirmed effective bioactivity and antibacterial properties with the hydroxyapatites sample doped with small amounts of Zn ions (less than 1%) [162, 163 and 164]. At a slightly higher concentration (1.3%), Zn ions shown to increase the level of osteoblast responses [165]. Studies on a hydroxyapatite doped with Zn were synthesized using the wet method and a hexahydrate Zn nitrate of Zn $(NO_3)_2 \cdot 6H_2O$ (wherein the Zn ion content was 1.6%), have shown its real impact on the reduction of S.aureus bacteria [166]. And other works also, its reported zinc incorporation to HA with antibacterial activity against K. pneumonia, proposed reason for the increase in antimicrobial activity against the bacterial strains may be due to the interaction between the nanocomposites and the bacterial cell membrane via the electrostatic attraction. This attraction leads to bacterial adhesion on the apatite surfaces. Similarly, the increase in bacterial adhesion with increasing zinc concentration leads to the inhibition of bacterial growth.

The size of the ZI was different according to the type of bacteria and the concentrations of Zn. Several factors have been attributed to the different response of Gram-positive and Gram-negative bacteria against Zn ions. These factors are different cell wall structure, membrane or the outer layer in each bacteria strain and different resistances to oxidant compounds and defense mechanisms to tackle oxidative stresses [167, 168].

The mechanism of action of Zn as an antibacterial agent is described to be similar to Ag ions. When Zn reaches the microbial cell membrane, it will be strongly adsorbed and penetrate into

the bacterial cell wall. The bacteria lose their proliferation capacity due to protein denaturation and the destruction that ultimately occurs [169]. Zn also has been reported to bind to the membranes of the microorganisms, consequently prolonging the lag phase of the growth cycle and increasing the generation time of the organisms, so that it takes each organism more time to complete the cell division [168].

Hybrid formulation of hydroxyapatite, which consists of mixing a common antibiotic with Zn ions, has been used to resolve the problem of local availability of the antibacterial agent and to provide a higher concentration of the antibiotic in the bone tissue [170]. In the mentioned work, hydroxyapatite was doped with Zn ions as carriers for the controlled release of ciprofloxacin, which exhibits antibacterial activity against S.aureus and Pseudomonas aeruginosa. It was shown that both the ciprofloxacin and Zn ions co-release. The Zn not only increases the total antibacterial activity, but also it resulted in a higher amount of ciprofloxacin release from the hybrid material as it reduces the crystallinity and increase the surface area of the nano grains. Using a similar formulation can result in higher efficiency of the therapy with lower doses of ciprofloxacin and a reduction in the formation of resistant strains.

CHAPTER FIVE

CONCLUSION AND RECOMMENDATION

In this study, synthesis of Hydroxyapatite (HA) by using egg shell as calcium precursor was done.in addition to enhance the property of the HA, ionic substitution to the HA that is zinc was substitution with different ratio. That's is from pure HA, 0.3-Zn-HA, 0.6-Zn-HA, 0.9-Zn-HA and 1.2-Zn-HA mol percent was substituted.

After the synthesis and acquiring of precipitates, characterization like XRD, FTIR, TGA and antibacterial test (Disc diffusion test) were done. Looking at the phase analysis by XRD, pure hydroxyapatite phase was observed for all samples including the zinc substituted. When calculating the crystal size of the samples, as the zinc ratio increased, the crystal size decreased inversely, and also the lattice parameter of "*a*" and "*c*" decease as concentration of zinc increased, this can imply zinc have been incorporated to the Hydroxyapatite.

The functional group was read from the FTIR data. Looking at the hydroxyl and PO_4, it was another input the material was indeed Hydroxyapatite. And also decrease in intensity at 1020-1120 cm^{-1}(v3) were characteristic to phosphate groups were observed as the zinc ratio increased that mean the crystal size decrement. The thermal analysis suggests that the decomposition temperature is around 733^oC. Therefore heat treatment of the precipitate is recommended at 450-500^oC.

The antibacterial test by disc diffusion showed that zone of inhibition increased as the zinc ratio increased. Which it can imply zinc substituted HA have an antibacterial property.

Generally, looking at the characterization analysis, zinc substituted at 1.2mol HA show satisfactory phase characteristic with high antibacterial activity

Therefore, as in the process of making HA, the waste materials egg shell is recycled, the cost for the production have decrease. Hence it may have a good hope for biomedical application in the future. It is recommended that this project idea be done with various synthesis routes, and zinc ratio to increase the yield in all prospects. And also it is known that carbon dioxide is greenhouse gas therefore, it is necessary to properly dispose or recycle this by product, after

calcination of the eggshell. So organic carbonate process for carbon dioxide that is, using propylene carbonate as an absorbent having selective or preferential solubility for carbon dioxide, by simple dissolution of the gas in the absorbent without chemically aliecting or reacting with the absorbent [172], can be a way to properly dispose the carbon dioxide for the safety of the environment.

REFERENCE

1. Bahrololooma ME et al. (2009) *Characterization of natural hydroxyapatite extracted from bovine cortical bone ash*. J Ceram Process Res 10:129–138
2. Sakka S, Bouaziz and J, Ayed FB. (2013) *Mechanical properties of biomaterials based on calcium phosphate and bioinert oxides for applications. Advances in biomaterials science and biomedical applications in Biomedicine*. Intech, Rijeka, 23–50.
3. Bohner M. (2000) *Calcium orthophosphates in medicine: from ceramics to calcium phosphate cements*. Injury4:37–47
4. Sellami I, Ayed and FB, Bouaziz J. (2000) *Effect of fluorapatite additive on the mechanical properties of tricalcium phosphatezirconia composites*. Mater Sci Eng 28(012029):1–8
5. Chaari K, et al. (2009) *elaboration and characterization of fluorapatite ceramic with controlled porosity*. Mater Chem Phys 113:219–226
6. Gutierres M, et al. (2007) *Opening wedge high tibial osteotomy using 3D biomodelling bonelike macroporous structures: case report.* J Mater Sci Mater Med 18:2377–2382
7. Takagi S, et al. (1987). *Enhanced enamel F uptake by monocalcium phosphate monohydrate gels.* J Dent Res66:1523–1526
8. Mulye NV and Turco SJ. (1994) *Use of dicalcium phosphate dihydrate for sustained release of highly water soluble drugs.* Drug Dev Ind Pharm20:2621–2632
9. Ribeiro DCDP, et al. (2012) *Study of the osteoconductive capacity of hydroxyapatite implanted into the femur of ovariectomized rats*. Microsc Res Tech 75:133–137
10. Jaramillo CD, et al. (2010) *Osteoconductive and osseointegration properties of a commercial hydroxyapatite compared to a synthetic product*. Rev Colomb Cienc Pecu 23:471–483
11. Itoh S, Kikuchi M, et al. (2001). *The biocompatibility and osteoconductive activity of a novel hydroxyapatite, collagen composite biomaterial, and its function as a carrier of rhBMP-2*. J Biomed Mater Res 54:445–453

12. Banks E, et al (1977*). Fibrous apatite grown on modified collagen*. Science 198:1164–1166
13. Fathi MH, et al (2008). *Preparation and bioactivity evaluation of bone-like hydroxyapatite nanopowder*. J Mater Process Tech202:536–542
14. Murray EJ and Messer HH (1981). *Turnover of bone zinc during normal and accelerated bone loss in rats*. J Nutr; 111:1641–7.
15. Bazin D, et al (2007). *Heavy elements in urinary stones*. Urol Res; 35:179–84.
16. Bazin D, et al (2008). *Very first tests on SOLEIL regarding the Zn environment in pathological calcifications made of apatite determined by X-ray absorption spectroscopy*. J Synchrotron Radiat; 15:506–9.
17. Windisch W (2001). *Homeostatic reactions of quantitative Zn metabolism on deficiency and subsequent repletion with Zn in Zn-65-labeled adult rats*. Trace Elem Electrolytes; 18:122–8.
18. Tvinnereim HM, et al (1999). *Zinc in primary teeth from children in Norway*. Sci Total Environ; 226:201–12.
19. Ito A, et al (2002). *Zinc releasing calcium phosphate for stimulating bone formation.* Mater Sci Eng; C22:21–5.
20. Ito A, et al (2000). *Preparation, solubility, and cytocompatibility of zinc-releasing calcium phosphate ceramics*. J Biomed Mater Res; 50:178–83.
21. Palmer LC and Newcomb CJ (2008). *Biomimetic systems for hydroxyapatite mineralization inspired by bone and enam*el. Chem Rev 108:4754–4783
22. Muhammad Akram (2014), *Rashid Ahmed et al. Extracting hydroxyapatite and its precursors from natural resources*. J Mater Sci 49:1461–1475
23. Sarah Shearman (2016) *Scotch egg company claims to have cracked problem of eggshell waste*. The Guardian, Guardian sustainable business
24. Williams, D.F.: (1999) *Williams's dictionary of biomaterials*, Liverpool University Press
25. Vallet-Regi, M., (2000), *Ceramics for Medical Applications*, the Royal Society of Chemistry, Dalton Transactions, pp. 97 – 108

26. Kweh, S. W. K. et al., (1999), *The Production and Characterization of Hydroxyapatite (HA) Powder, Journal of Materials Processing Technologies,* Vol. 89-90, pp. 373 – 377
27. Koutsopoulos, S. et al., (2002), *Synthesis and Characterization of Hydroxyapatite Crystals: A Review Study on the Analytical Methods,* Wiley Periodicals, Inc.
28. Weiner, S. and Wagner, H. D., (1998), *―The Material Bone: Structure-Mechanical Function Relations‖, Annual Review of Materials Science*, Vol. 28, pp. 271 – 298
29. Hellmich, C. and Ulm, F. J., (2002), *―Micromechanical Model for Ultrastructural Stiffness of Mineralized Tissues‖, Journal of Engineering*. Mech., Vol. 128, Issue 8, pp. 898 – 908
30. Rho, J. Y. et al., (1998), *―Mechanical Properties and the Hierarchical Structure of Bone‖, Medical Engineering Physics*, Vol. 20, pp. 92 – 102
31. Liu, Y., et al., (2005), *―BMP-2 Liberated from Biomimetic Implant Coatings Induces and Sustains Direct Ossification in an Ectopic Rat Model*. Bone, Vol. 36, pp. 745 – 757
32. Martin, R. B. et al., (1998), *Skeletal Tissue Mechanics*, Springer-Verlag, New York, ISBN: 0-387-98474-7
33. Burger, E. H., (2001), *―Experiments on Cell Mechanosensitivity: Bone Cells as Mechanical Engineers‖, In: Bone Mechanics Handbook.* Cowin SC (ed). CRC Press, New York.
34. Orlovskii, V. P. et al., (2002), *―Hydroxyapatite and Hydroxyapatite-Based Ceramics‖*, Inorganics Materials, Vol. 38, pp. 973 – 984
35. Puajindanetr, S., (1993), *―Characterization and Sintering of Precipitated Hydroxyapatite‖*, Ph.D. Thesis, Queen Mary and Westfield College London, Great Britain
36. Brown, P. A, (1994), *Hydroxyapatite and Related Materials*, CRC Press, Inc., ISBN: 0 - 8493 - 4750 – 5

37. Slosarczyk, A. et al., (2005), *FTIR and XRD Evaluation of Carbonated Hydroxyapatite Powders Synthesized by Wet Methods*. Journal of Molecular Structure, Volumes 744-747, pp. 657 – 661
38. Zhu, X., (2005), ―*Nano Hydroxyapatite/Collagen, Nano Hydroxyapatite and Anodic Oxides on Titanium – Preparation, Characterization and Biological Response*‖. Inaugural Dissertation, Medical Faculty, Eberhard-Karls-University
39. Young, R. A. and Holcomb, D. W., (1982). *Variability of Hydroxyapatite Preparations*. Calcified Tissue International, Vol. 34, pp. 17 – 32
40. Cheang, P. and Khor, K. A., (1996), *Addressing Processing Problems Associated with Plasma Coating of Hydroxyapatite Coatings*, Biomaterials, Vol. 17, pp. 537 – 544
41. Raynaud, S. et al., (2002), *Calcium Phosphate Apatite's with Variable Ca/P Atomic Ratio I., Synthesis, Characterization and Thermal Stability of Powders*, Biomaterials, Vol. 23, pp. 1065 –1072
42. Liu, J. et al., (2003), *The Influence of pH and Temperature on the Morphology of Hydroxyapatite Synthesized by Hydrothermal Method*, Ceramics International, Vol. 29, pp. 629 – 633
43. Suchanek, W. and Yoshimura, M., (1998), *Processing and Properties of Hydroxyapatite-Based Biomaterials for use as Hard Tissue Replacement Implants*, Journal of Materials Research, Vol. 13, pp. 94 – 114
44. Kehoe, S., (2008), ―*Calcium Phosphates for Medical Applications*‖, Dublin City University, J. Stokes, Ed., Materials Processing Research Centre, Materials Processing Research, ISBN 1 87232-752-X
45. Rhee, S. H., (2002), *Synthesis of Hydroxyapatite via Mechanochemical Treatment*, Biomaterials, Vol. 23, pp. 1147 – 1152
46. Zhang, H. et al., (2002), ―*Morphology and Formation Mechanism of Hydroxyapatite Whiskers from Moderately Acid Solution*‖, Materials Research, Vol. 6, pp. 111 – 115
47. H.W. Kim, et al (2004). *Strontium substituted calcium phosphate biphasic ceramics obtained by a powder precipitation method*, J. Mater. Sci.-Mater. Med 15 1129–1134.

48. J.M. Hughes and J. Rakovan (2002), *The crystal structure of apatite, Ca5(PO4)3(F, OH, Cl), in: M.J. Kohn, J. Rakovan, J.M. Hughes (Eds.), Phosphates: Geochemical, Geobiological and Material Importance, Reviews in Mineralogy and Geochemistry, vol. 48,* Mineralogical Society of America, Washington, DC, , pp. 1–12.
49. H. El Feki, et al (2000). *Studies by thermally stimulated current (TSC) of hydroxyl and fluoro-carbonated apatites containing sodium ions*, J. Phys. Condens. Matter 12 8331–8343.
50. E.A.P. De Maeyer, et al (1993). *Effect of heating on the constitution of Naþ and CO32 containing apatites obtained by hydrolysis of monetite*, Inorg. Chem. 33 5999–6006.
51. H. El Feki, et al. (2000), *Localization of potassium in substituted lead hydroxyapatite: Pb9.30K0.60(PO4)6(OH)1.20 by X-ray diffraction*, Solid State Sci. 2 725–733.
52. A. Nounah, J.et al. (1992), Localization of cadmium in cadmium-containing hydroxy- and fluorapatites, J. Alloys Compd. 188 141–146.
53. H. El Feki, et al. (1999) , *Structure refinements by the Rietveld method of partially substituted hydroxyapatite: Ca9Na0.5 (PO4)4.5(CO3)1.5(OH)2*, J. Alloys Compd. 287 114–120
54. A. Bigi, et al. (2007), *Strontium-substituted hydroxyapatite nanocrystals*, Inorg. Chim. Acta 360 1009–1116.
55. M. Wakamura, et al (2000). , *Surface structure and composition of calcium nhydroxyapatites substituted with Al(III), La(III) and Fe (III) ions*, Colloid Surf. A—Physicochem. Eng. Asp 164 297–305.
56. S. Kannan, et al (2005). *Synthesis and characterization of magnesium substituted biphasic mixtures of controlled hydroxyapatite/β-tricalcium phosphate ratios*, J. Solid State Chem. 178 3190–3196.
57. E. Landi, , et al (2006)., *Biomemitic Mg- and Mg, CO3-substituted hydroxyapatites: synthesis characterization and in vitro behavior*, J. Eur. Ceram. Soc. 26 2593–2601.

58. I.R. Gibson and W. Bondfield (2002), *Preparation and characterization of Mg/ carbonate co-substituted hydroxyapatites*, J. Mater. Sci.-Mater. Med. 13 685–693.
59. W. Acchar and E.G. Ramalho (2008), *Effect of MnO2 addition on sintering behavior of tricalcium phosphate: premilinary results*, Mater. Sci. Eng. C 28 248–252.
60. M. Li, et al. (2008), *Structural characterization of zinc-substituted hydroxyapatite prepared by hydrothermal method*, J. Mater. Sci.-Mater. Med 19 797–803.
61. K. Niespodziana, et al (2010), *Fabrication and properties of titanium–hydroxyapatite nanocomposites*, Mater. Chem. Phys. 123 160–165.
62. Y. Sogo, T. Sakurai, et al. (2002), *The most appropriate (Ca+Zn)/P molar ratio to minimize the zinc content of ZnTCP/HAP ceramic used in the promotion of bone formation*, J. Biomed. Mater. Res. 62 457–463.
63. A. Ito, K. Ojima, et al (2000) *Preparation, solubility, and cytocompatibility of zinc-releasing calcium phosphate ceramics*, J. Biomed. Mater. Res. 50 178–183.
64. E. Fujii, M. Ohkubo, et al (2006) *Selective protein adsorption property and characterization of nano-crystalline zinc containing hydroxyapatite*, Acta Biomater. 2 69–74.
65. Y. Tang, H.F. et al (2009) Zinc *incorporation into hydroxylapatite*, Biomaterials 30 2864–2872.
66. A. Ito, H. Kawamura, et al (2002) *Zinc-releasing calcium phosphate for stimulating bone formation*, Mater. Sci. Eng. C 22 21–25.
67. F. Miyaji, et al *Formation and structure of zinc substituted calcium hydroxyapatite*, Mater. Res. Bull. 40 (2005) 209–220.
68. A. Bigi, E. et al (1995) *Inhibiting effect of zinc on hydroxylapatite crystallization*, J. Inorg. Biochem. 58 49–58.
69. S. Hayakawa, et al (2007)., *Structural characterization and protein adsorption property of hydroxyapatite particles modified with zinc ions*, J. Am. Ceram. Soc. 90 565–569.
70. R.J. Chung, et al (2006) *Antimicrobial effects and human gingival biocompatibility of hydroxyapatite sol–gel coatings*, J. Biomed. Mater. Res. 76B 169–178.

71. G. Suresh Kumar , et al. (2012), *Synthesis, characterization and in vitro studies of zinc and carbonate co-substituted nano-hydroxyapatite for biomedical applications*, Mater. Chem. Phys. 134 1127–1135.
72. N. Kanzaki, et al (2000) *Inhibitory effect of magnesium and zinc on crystallization kinetics of hydroxyapatite (0 0 0 1) face*, J. Phys. Chem. B 104 4189 4194.
73. F. Ren, R. Xin, X. Ge, Y. Leng, (2009) Characterization and structural analysis of zinc substituted hydroxyapatites, Acta Biomater. 5 3141–3149.
74. J. Terra, M. Jiang, D.E. Ellis, (2002) *Characterization of electronic structure and bonding in hydroxyapatite: Zn substitution for Ca, Philos*. Mag. A 82 2357–2377.
75. K. Matsunaga, (2008) *First-principles study of substitutional magnesium and zinc in hydroxyapatite and octacalcium phosphate*, J. Chem. Phys. 128 245101.
76. H. Chappell, D. Shepherd, S. (2009) *Best, Zinc substituted hydroxyapatite—a comparison of modeling and experimental data*, Key Eng. Mater. 396– 398 729–732.
77. T. Tamm, M. Peld, (2006) Computational *study of cation substitutions in apatites*, J. Solid State Chem. 179 1581–1587.
78. Y. Sogo, T. Sakurai, K. Onuma, et al. (2002), *The most appropriate (CaþZn)/P molar ratio to minimize the zinc content of ZnTCP/HAP ceramic used in the promotion of bone formation*, J. Biomed. Mater. Res. 62 () 457–463.
79. Feki HC, et al (1991) *Carbonate ions in apatites: infrared investigations in the ly 4 CO3 domain*. Calcif Tissue Int 49:269–274
80. Rivera EM, et al (1999) *Synthesis of hydroxyapatite from eggshells*. Mater Lett 41:128–134
81. Belcher AM, et al (1996) *Control of crystal phase switching and orientation by soluble mollusc-shell proteins.* Nature 381:56–58
82. Kaplan DL (1998) Mollusc Dhell *structures: novel design strategies for synthetic materials*. Science 3:232–236
83. Xu G, et al (2001) *Continuous crystalline carbonate apatite thin films. a biomimetic approach.* J Am Chem Soc 123:2196–2203

84. Baig AA, et al (1996) *Effect of carbonate content and crystallinity on the metastable equilibrium solubility behavior of carbonated apatites.* J Colloid Interface Sci 179:608–617
85. Nelson DGA, et al (1983) *Effect of carbonate and fluoride on the dissolution behaviour of synthetic apatites*. Caries Res 17:200–211
86. Landi E, et al (2003) *Carbonated hydroxyapatite as bone substitute*. J Eur Ceram Soc 23:2931–2937
87. Lee SJ and Oh SH (2003) *Fabrication of calcium phosphate bioceramics by using eggshell and phosphoric acid*. Mater Lett 57:4570–4574
88. de Paula SM, et al (2010) *Confocal Raman and electronic microscopy studies on the topotactic conversion of calcium carbonate from Pomacea lineateshells into hydroxyapatite bio ceramic materials in phosphate media*. Micron 41:983–989
89. Murugan R, Ramakrishna S (2004) *Crystallographic study of hydroxyapatite bio ceramics derived from various sources*. Crys Growth Des 5:111–112
90. Kim YH, et al (2005) *Preparation of porous Si incorporated hydroxyapatite*. Curr Appl Phys 5:538–541
91. Nayar S, Guha A (2009) *Waste utilization for the controlled synthesis of nanosized hydroxyapatite*. Mat Sci Eng C-Mater 29:1326–1329
92. Krishna DSR, et al (2007) *A novel route for synthesis of nanocrystalline hydroxyapatite from eggshell waste*. J Mater Sci Mater Med 18:1735–1743
93. Sanosh KP, et al (2009) *Utilization of bio-waste eggshells to synthesize nanocrystalline hydroxyapatite powders*. Mater Lett 63:2100–2102
94. Habib F, et al (2012) *Synthesis route and characterization of hydroxyapatite powder prepared from waste egg shells*. J Chem Pak 34:584–588
95. Kumar GS, et al (2012) *Microwave conversion of eggshells intoflower like hydroxyapatite nanostructure for biomedical applications*. Mater Lett 76:198–200
96. Goloshchapov DL, et al (2013) *Synthesis of nanocrystalline hydroxyapatite by precipitation using hen's eggshell*. Ceram Int 39:4539–4549
97. Wu SC et al (2011) *Hydroxyapatite synthesized from oyster shell powders by ball milling and heat treatment.* Mater charact 62:1180–1187

98. Zhang Y, et al (2011) *Conversion of egg-shell to hydroxyapatite for highly sensitive detection of endocrine disruptor bisphenol A*. J Mater Chem 21:14428–14431

99. Wu SC, et al (2013) *a hydrothermal synthesis of eggshell and fruit waste extract to produce nanosized hydroxyapatite*. Ceram Inter. doi:10.1016/j. ceramint.2013.03.094

100. Ho WF, et al (2013) *Calcium phosphate bio ceramics synthesized from eggshell powders through a solid state reaction*. Ceram Inter. doi:10.1016/j. ceramint.2013.01.076

101. Shariffuddin JH, et al (2013) *Greener photo catalysts: hydroxyapatite derived from waste mussel shells for the photocatalytic degradation of a model azo dye wastewater*. Chem Eng Res Des. doi:10.1016/j.cherd.2013.04.018

102. Meski S, et al (2010) *Removal of Lead Ions by Hydroxyapatite Prepared from the Egg Shel*. J Chem Eng Data 55:3923–3928

103. Li S, et al (2012) *Conversion of calcined eggshells into flower-like hydroxyapatite agglomerates by solvothermal method using hydrogen peroxide, N, N dimethylformamide mixed solvents*. J Am Ceram Soc 95:3377–3379

104. A´ lvarez-Lloret P, et al (2010) *Crystallographic control of the hydrothermal conversion of calcitic sea urchin spine (Paracentrotus lividus) into apatite*. Crys Growth Des 10:5227–5232

105. Villarreal NE, et al (2012) *Biomaterials from agricultural waste: eggshell-based hydroxyapatite.* Water Air Soil Pollut 223:3643–3646

106. Chaudhuri B, et al. (2013) *Preparation and characterization of nanocrystalline hydroxyapatite from egg shell and K_2HPO_4solution*. Mater Lett 97:148–150

107. Morgan, H. et al., (2000), ―*Preparation and Characterisation of Monoclinic Hydroxyapatite and its Precipitated Carbonate Apatite Intermediate*‖, Biomaterials, Vol. 21, Issue 6, pp. 617 – 627

108. Nadir, S. et al., (1996), ―*Synthèse par Neutralisation d'une Hydroxyapatite Pure à Partir de L'acide Orthophosphorique Technique et de la Calcite*‖, Phosphorus Sulfur and Silicon, Vol. 112, pp. 33 – 40

109. SRM2910, (2003), ―*Certificate of Analysis for Standard Reference Material (SRM2910: Calcium Hydroxyapatite*)‖ National Institute of Standards Technology, SRM Program, Gaithersburg, MD 20899, U.S.A, pp. 1 – 9

110. Calderin, L. et al., (2005), ―*A Shell Model of the Lattice Dynamics of Hydroxyapatite*‖, Physics Review: B, Vol. 72, pp. 224304-16

111. Haverty, D. et al., (2005), ―*Structure and Stability of Hydroxyapatite: Density Functional Calculation and Rietveld Analysis*‖, Physics Review: B, Vol. 71, pp. 094103 – 9

112. Corno. M., (2006), ―*Periodic* ab initio *Study of Structural and Vibrational Features of Hexagonal Hydroxyapatite, Ca10(PO4)6(OH)2*‖, Phys. Chem. Chem. Phys., Vol. 8, pp. 2464 – 2472

113. Kumar. R. et al., (2001), *RF Plasma Processing of Ultra-Fine Hydroxyapatite Powders*, Journal of Materials Processing Technology, Volume 113, Issues 1-3, pp. 456 – 462

114. LeGeros, R. Z. et al., (1982), ―*The Effect of Fluoride on the Stability of Synthetic and Biological (Bone) Mineral Apatites*‖, In: Menczel J, Robin GC, Makin M, Steinbeg R, editors. Osteoporosis. New York: Wiley; pp. 327 – 341

115. Elliott, J., (1994), ―*Structure and Chemistry of Apatites and Other Calcium Orthophosphates*‖, Amsterdam, Elsevier

116. Lazic, S. et al., (2001), *The effect of Temperature on the Properties of Hydroxyapatite Precipitated from Calcium Hydroxide and Phosphoric Acid*, Thermochimica Acta, Vol. 374, pp. 13 – 22

117. Thomas, K. A. et al., (1985), ―*An Evaluation of Variables Influencing Implant Fixation by Direct Bone Apposition*‖, Journal of Biomedical Materials Research, Vol. 19, pp. 875 – 901

118. Seckler, M. M. et al., (1999), *Influence of Process Conditions on Hydroxyapatite Crystallinity Obtained by Direct Crystallization*, Materials Research, Vol. 2, No. 2, pp. 59 – 62

119. Mostafa, N. Y., (2005), ―*Characterization, Thermal Stability and Sintering of Hydroxyapatite Powders Prepared by Different Routes*‖, Materials Chemistry and Physics, Vol. 94, Issues 2 – 3, pp. 333 – 341

120. Luo, P. and Nieh, T. G., (1995), *Synthesis of Ultrafine Hydroxyapatite Particles by a Spray Dry Method*, Materials Science & Engineering: C3, pp. 75 – 78

121. Afshar, A. et al., (2003), *Some Important Factors in the Wet Precipitation of Hydroxyapatite*, Materials and Design, Vol. 24, pp. 197 – 202

122. Smiciklas, I. et al., (2005), *Experimental Design Approach in the Synthesis of Hydroxyapatite by Neutralization Method*, Separation and Purification Technology, Volume 44, Issue 2, pp. 97 – 102

123. Giulietti, M. et al., (2001), *Industrial Crystallisation and Precipitation from Solutions: State of the Technique*, Brazilian Journal of Chemical Engineering, Vol. 15, Issue 4, pp. 423 – 440

124. Pang, Y. X. et al., (2003), *Influence of Temperature, Ripening Time and Calcination on the Morphology and Crystallinity of Hydroxyapatite Nanoparticles*, Journal of the European Ceramic Society, Vol. 23, pp. 1697 – 1704

125. Bouyer, E., (2000), ―*Morphological Study of Hydroxyapatite Nanocrystal Suspension*‖, *Journal of Materials Science*: Materials in Medicine, Vol. 11, pp. 523 – 531

126. Aizawa, M. et al., (2006), ―S*yntheses of Calcium - Deficient Apatite Fibers by a Homogeneous Precipitation Method and their Characterizations*‖, Journal of the European Ceramic Society, Vol. 26, pp. 501 – 507

127. Knowles, J. C., (2000), ―*Characterization of the Rheological Properties and Zeta Potential of a Range of Hydroxyapatite Powders*‖, Biomaterials, Vol. 21, pp. 1387 – 1392

128. Suchanek W and Yoshimura M. (1998) *Processing and properties of hydroxyapatite-based biomaterials for use as hard tissue replacement implants*. J MaterRes.;13(1):94-117

129. Widmer AF.9 2001) *New developments in diagnosis and treatment of infection in orthopedic implants*. Clin Infect Dis.;1(33):S94-106.

130. Anthony R, et al (1999). *Prosthetic joint infection. Current Infectious Diseases Reports*. Current Infectious Diseases Reports.; 1(3):267-272.

131. Collins D and McKenzie J (1991). *Infections at the site of a hip implant*. Clinical Orthopaedics.; 269:9-15.

132. Tattevin P,et al (1999). *Prosthetic joint infection: when can prosthesis salvage be considered?* Clin Infect Dis.; 2:292-295.

133. Goldenberg D. (1998) *Septic arthritis*. The Lancet.; 351:197-202.

134. Ribeiro M,et al (2012). *Infection of orthopedic implants with emphasis on bacterial adhesion process and techniques used in studying bacterial-material interactions.* Biomatter.;2(4):176-194.

135. Goodman S, et al (2013). *The future of biologic coatings for orthopaedic implants.* Biomaterials. 34(13):3174-3183.

136. Petrosillo N. (2013) *Epidemiology of Infections in the New Century. In: Signore A, Quintero A, editors. Diagnostic Imaging of Infections and Inflammatory Diseases:* John Wiley & Sons, Inc.;. p. 1-14.

137. Uçkay I,et al. (2013) *Bacterial Osteomyelitis: The Clinician's Point of View. Diagnostic Imaging of Infections and Inflammatory Diseases*: John Wiley & Sons, Inc.;. p. 15-26.

138. David MZ and Daum RS (2010). *Community-Associated Methicillin-Resistant Staphylococcus aureus: Epidemiology and Clinical Consequences of an Emerging Epidemic*. Clin Microbiol Rev.;23(3):616-687.

139. Goyal N, et al. (2013) *Instructional review: general orthopaedics Methicillin-resistant Staphylococcus aureus (MRSA).* Bone Joint J.;95(B):4-9.

140. Hanssen A. (2005) *Local antibiotic delivery vehicles in the treatment of musculoskeletal infection*. Clin Orthop Relat Res. (437):91-96.

141. . Visurraga J, et al (2011). *Metal nanostructures as antibacterial agents. Science against microbial pathogens*: communicating current research and technological advances..

142. Hajipour M, et al (2012). *Antibacterial properties of nanoparticles,. Trends in Biotechnology,*; 30(10):499- 511.

143. Kandile N, et al. (2010) *Silver Nanoparticles Effect on Antimicrobial and Antifungal Activity of New Heterocycles*. Bull Korean Chem Soc.; 31(12).

144. Li M, et al. (2008). *Structural characterization of zinc-substituted hydroxyapatite prepared by hydrothermal method*. J Mater Sci Mater Med.;19(2):797-803.

145. Stanic V, et al. (2010) *Synthesis, characterization and antimicrobial activity of copper and zinc- doped hydroxyapatite nanopowders*. Applied Surface Science.; 256(20):6083-6089.

146. Wolschendorf F, et al. (2011) *Copper resistance is essential for virulence of Mycobacterium tuberculosis*. Proc Natl Acad Sci U S A.; 108(4):1621-1626.

147. Yang Y, Zhang L, Xu K. *Effect of storing on the microstructure of Ag/Cu/HA powder*. Ceramics International. 2009; 35(4):1595-1601.

148. Kawamura H, et al. (2000) *Stimulatory effect of zinc-releasing calcium phosphate implant on bone formation in rabbit femora*. J Biomed Mater Res.; 50(2):184-190.

149. Grandjean-Laquerriere et al (2006). *Influence of the zinc concentration of sol-gel derived zinc substituted hydroxyapatite on cytokine production by human monocytes in vitro*. Biomaerials.; 27(17):6.

150. Suryanarayana C, Grant Norton M. X-Ray Diffraction: A Practical Approach. Illustrated ed: Springer; 1998

151. Cullity B, Stock S. (2001) *Elements of X-Ray Diffraction.* 3, *Illustrated ed*: Prentic Hall;.

152. Ferraro J, Krishnan K. (2012) *Practical Fourier transform infrared spectroscopy:*

Industrial and laboratory chemical analysis *San Diego*: Elsevier;.

153. Meenan B, et al (2000) *Thermal analysis studies of poly(etheretherketone)/hydroxyapatite biocomposite mixtures*. J Mater Sci.;11(8):481-490.

154. Sandrine Gomes et al. (2012) .*On the effect of temperature on the insertion of zinc into hydroxyapatite*. Acta Biomaterialia 8.1180–1189

155. Liga Berzina-Cimdina and Natalija Borodajenko (2012). *Research of Calcium Phosphates Using Fourier Transform Infrared Spectroscopy, Infrared Spectroscopy-Materials Science, Engineering and Technology, Prof. Theophanides Theophile* (Ed.), ISBN: 978-953-51-0537-4

156. REN Fuzeng (2008) *Synthesis and Characterization of Nanocrystalline Zn, Mg Substituted Hydroxyapatite. Unpublished''* Thesis Submitted to the Hong Kong University of Science and Technology. 43pp

157. P. N.Kumta, et al., (2005) Nanostructured calcium phosphates for biomedical *applications: novel synthesis and characterization.* Acta Biomaterialia, (1): p. 65-83.

158. Nagarajan P, Rajagopalan V. (2008) *Enhanced bioactivity of ZnO nanoparticles—an antimicrobialstudy.* J Sci Technol Adv Mater.;9(3).

159. Zakaria Z, et al (2010). *Lack of antimicrobial activities of Dicranopteris linearisextracts and fractions*. Afr J Microbial.;4(2):071-075.

160. Toshiaki O, et al (2008) *Antibacterial activity of ZnO powder with crystallographic orientation.* J Mater Sci Mater Med.;19(3):1407-1413.

161. Matei A, et al (2008). *Synthesis and characterization of ZnO – polymer nanocomposites.* Int J Mater Form.;1(1):767-770.

162. Ohsumi Y, et al. (1988) *Changes induced in the permeability barrier of the yeast plasma membrane by cupric ion*. J Bacteriol.;170(6):2676-2682.

163. Yang Y, et al (2009). *Effect of storing on the microstructure of Ag/Cu/HA powder.Ceramics International*.;35(4):1595-1601.

164. Kawamura H, et al. (2000) Stimulatory effect of zinc-releasing calcium phosphate implant on bone formation in rabbit femora. J Biomed Mater Res.;50(2):184-190.

165. Webster T, et al (2004) *Osteoblast response to hydroxyapatite doped with divalent and trivalent cations. Biomaterials*. 2004;25(11):2111-2121.

166. Thian E, et al (2013). *Zinc-substituted hydroxyapatite: a biomaterial with enhanced, bioactivity and antibacterial properties*. J Mater Sci Mater Med. 2013;24(2):437-445.

167. Reddy K, Kevin F, Jason B, Denise G, Cory H, Alex P. Selective toxicity of zinc oxide nanoparticles to prokaryotic and eukaryotic systems. J Appl Phys Lett. 2007; 90(21):1-4.

168. Selahattin A, et al (1998). *The effect of zinc on microbial growth. Tr* J Med Sci.;28:595-597.

169. Sun T, et al (2014). *Preparation and antibacterial properties of titanium-doped ZnO from different zinc salts*. Nanoscale Res Lett. 2014/02/27; 9(1):1-11.

170. Venkatasubbu G et al (2011). *Nanocrystalline hydroxyapatite and zinc doped hydroxyapatite as carrier material for controlled delivery of ciprofloxacin*. 3 Biotech. ;1(3):173-186.

171. Cullity B, Stock S. (2001). *Elements of X-Ray Diffraction*. 3, Illustrated ed: Prentic Hall; p-392

172. Arthur L Kohl and Frederick E Miller (1960), *Organic carbonate process for carbon dioxide*. US2926751A